

# Metallography and Microstructures of Cast Iron

Janina M. Radzikowska, The Foundry Research Institute, Kraków, Poland

CAST IRON is an iron-carbon cast alloy with other elements that is made by remelting pig iron, scrap, and other additions. For differentiation from steel and cast steel, cast iron is defined as a cast alloy with a carbon content (min 2.03%) that ensures the solidification of the final phase with a eutectic transformation. Depending on chemical specifications, cast irons can be nonalloyed or alloyed. Table 1 lists the range of compositions for nonalloyed cast irons (Ref 1). The range of alloyed irons is much wider, and they contain either higher amounts of common components, such as silicon and manganese, or special additions, such as nickel, chromium, aluminum, molybdenum, tungsten, copper, vanadium, titanium, plus others.

Free graphite is a characteristic constituent of nonalloyed and low-alloyed cast irons. Precipitation of graphite directly from the liquid occurs when solidification takes place in the range between the temperatures of stable transformation ( $T_{st}$ ) and metastable transformation ( $T_{mst}$ ), which are, respectively, 1153 °C (2107 °F) and 1147 °C (2097 °F), according to the iron-carbon diagram. In this case, the permissible undercooling degree is  $\Delta T_{max} = T_{st} - T_{mst}$ . In the case of a higher undercooling degree, that is, in the temperatures below  $T_{mst}$ , primary solidification and eutectic solidification can both take place completely or partially in the metastable system, with precipitation of primary cementite or ledeburite. Graphitization can also take place in the range of critical temperatures during solid-state transformations. The equilibrium of phases  $Fe_{\gamma} = Fe_{\alpha} + Fe_3C$

occurs only at the temperature  $723 \pm 2$  °C (1333 ± 4 °F), while equilibrium of phases  $Fe_{\gamma} = Fe_{\alpha} + C_{gr}$  occurs at the temperature  $738 \pm 3$  °C (1360 ± 5 °F). So, in the range of temperatures 738 to 723 °C (1360 to 1333 °F), the austenite can decompose only into a mixture of ferrite with graphite instead of with cementite (Ref 2).

The previous considerations regard only pure iron-carbon alloys. In cast iron, which is a multicomponent alloy, these temperatures can be changed by different factors: chemical composition, ability of cast iron for nucleation, and cooling rate. Silicon and phosphorus both strongly affect the carbon content of the eutectic. That dependence was defined as a carbon equivalent ( $C_e$ ) value that is the total carbon content plus one-third the sum of the silicon and phosphorus content (Ref 2). Cast iron, with a composition equivalent of approximately 4.3, solidifies as a eutectic. If the  $C_e$  is >4.3, it is hypereutectic; if it is <4.3, cast iron is hypoeutectic (Ref 3).

Eutectic cells are the elementary units for graphite nucleation. The cells solidify from the separate nuclei, which are basically graphite but also nonmetallic inclusions such as oxides and sulfides as well as defects and material discontinuities. Cell size depends on the nucleation rate in the cast iron. When the cooling rate and the degree of undercooling increase, the number of eutectic cells also increases, and their microstructure changes, promoting radial-spherical shape (Ref 2).

## Preparation for Microexamination

Preparation of cast iron specimens for microstructural examination is difficult due to the need to properly retain the very soft graphite phase, when present, that is embedded in a harder matrix. Also, in the case of gray irons with a soft ferritic matrix, grinding scratches can be difficult to remove in the polishing process. When shrinkage cavities are present, which is common, the cavities must not be enlarged or smeared over.

Retention of graphite in cast iron is a common polishing problem that has received considerable

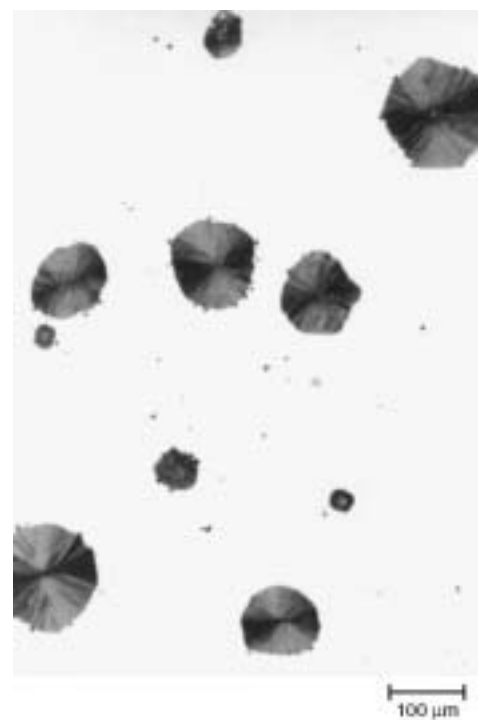


**Table 1 Range of chemical compositions for typical nonalloyed and low-alloyed cast irons**

Type of iron	Composition, %				
	C	Si	Mn	P	S
Gray (FG)	2.5–4.0	1.0–3.0	0.2–1.0	0.002–1.0	0.02–0.025
Compacted graphite (CG)	2.5–4.0	1.0–3.0	0.2–1.0	0.01–0.1	0.01–0.03
Ductile (SG)	3.0–4.0	1.8–2.8	0.1–1.0	0.01–0.1	0.01–0.03
White	1.8–3.6	0.5–1.9	0.25–0.8	0.06–0.2	0.06–0.2
Malleable (TG)	2.2–2.9	0.9–1.9	0.15–1.2	0.02–0.2	0.02–0.2

FG, flake graphite; SG, spheroidal graphite; TG, tempered graphite. Source: Ref 1

**Fig. 1** Spheroidal graphite in as-cast ductile iron (Fe-3.7%C-2.4%Si-0.59%Mn-0.025%P-0.01%S-0.095%Mo-1.4%Cu) close to the edge of the specimen, which was 30 mm (1.2 in.) in diameter. The specimen was embedded. As-polished. 100 ×

attention. Coarse grinding is a critical stage, so, if the soft graphite is lost during coarse grinding, it cannot be recovered in subsequent steps and

will be seen as an open or collapsed cavity. Silicon carbide (SiC) grinding papers are preferred to emery, because SiC cuts efficiently, while emery paper does not, and SiC produces less damage.

Fresh paper should always be used; never grind with worn paper. White iron, by contrast, contains extremely hard iron carbides that resist abrasion and tend to remain in relief above the softer matrix after polishing (Ref 4).

Quality-control studies, based on image analysis measurements of the amount of phases and the graphite shape and size, also need perfectly prepared specimens with fully retained graphite phase and with microstructural constituents correctly revealed by etching.

**Specimen Preparation.** The metallographic specimen preparation process for microstructural investigations of cast iron specimens usually consists of five stages: sampling, cold or hot mounting, grinding, polishing, and etching with a suitable etchant to reveal the microstructure. Each stage presents particular problems in the case of cast iron. Of course, the graphite phase is studied after polishing and before etching.

**Sampling** is the first step—selecting the test location or locations to be evaluated metallographically. Usually, cast iron castings have a considerable variation in microstructure between surface and core. Selection of the test location is very important to obtain representative results from the microstructural examination. Samples can be obtained by cutting them out from either a large or small casting or from standard test bars, such as microslugs, ears, or keel bars; however, the microstructure of these pieces may not be representative for the actual casting due to substantial differences in the solidification rates. Production saws, such as large, abrasive cutoff saws, band saws, or power hacksaws, can be used for dividing medium-sized casting into smaller samples. In the case of very large castings, flame cutting may be used. Next, the pieces

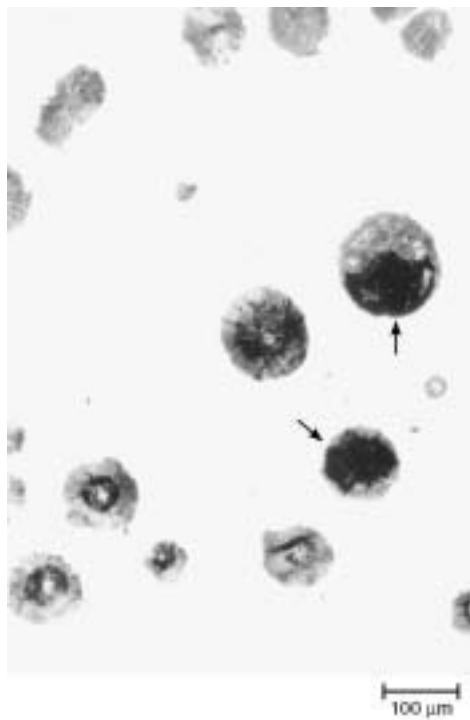


**Fig. 2** Same as-cast ductile iron as in Fig. 1, but the specimen was not embedded. The arrows show the pulled-out graphite. As-polished. 100×



**Fig. 4** Same as in Fig. 3 but close to the center of the specimen. As-polished. 100×

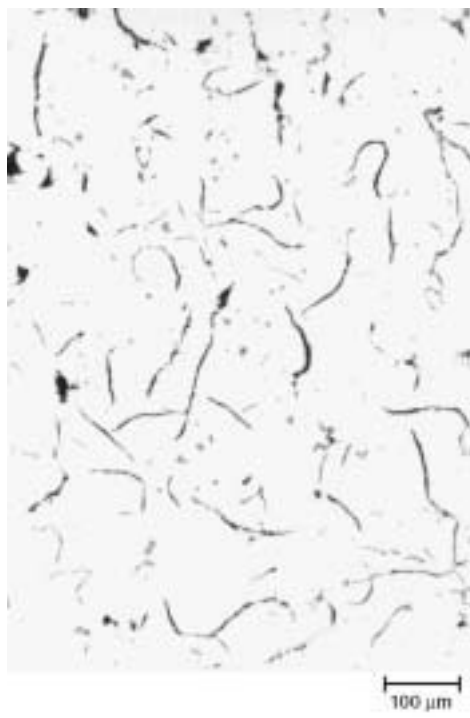


**Fig. 3** Flake graphite in as-cast gray iron (Fe-3.5% C-2.95% Si-0.40% Mn-0.08% P-0.01% S-0.13% Ni-0.15% Cu) close to the edge of the unembedded specimen, which was 30 mm (1.2 in.) in diameter. As-polished. 100×

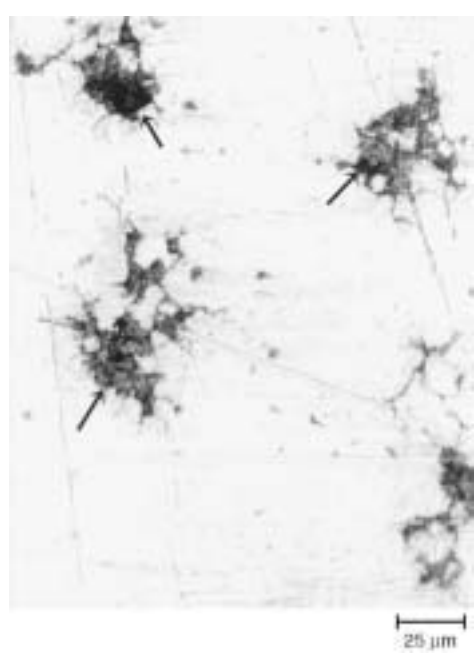


**Fig. 5** Temper graphite in malleable iron (Fe-2.9% C-1.5% Si-0.53% Mn-0.06% P-0.22% S-0.08% Ni-0.1% Cu-0.09% Cr-0.003% Bi) after grinding on P1000 SiC waterproof paper. The casting was annealed at 950 °C (1740 °F), held 10 h, furnace cooled to 720 °C (1330 °F), held 16 h, and air cooled. The arrows show the pulled-out graphite. As-polished. 400×

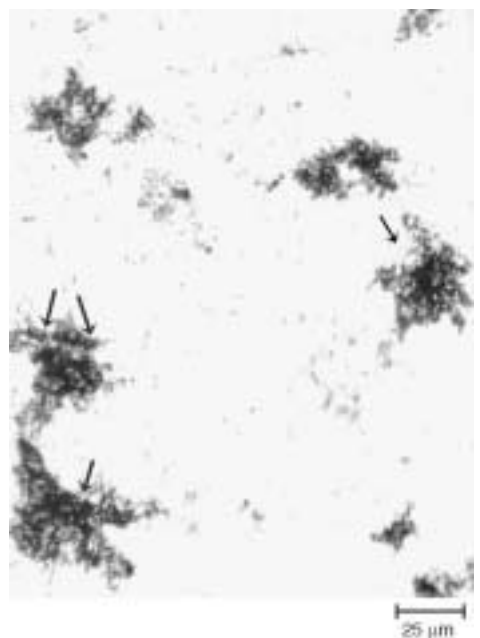


**Fig. 6** Same as in Fig. 5 but after polishing with 9 μm diamond suspension. The arrows show the pulled-out graphite. As-polished. 400×

can be reduced to the desired size for metallographic specimens by using a laboratory abrasive cutoff saw or a band saw. If the casting was

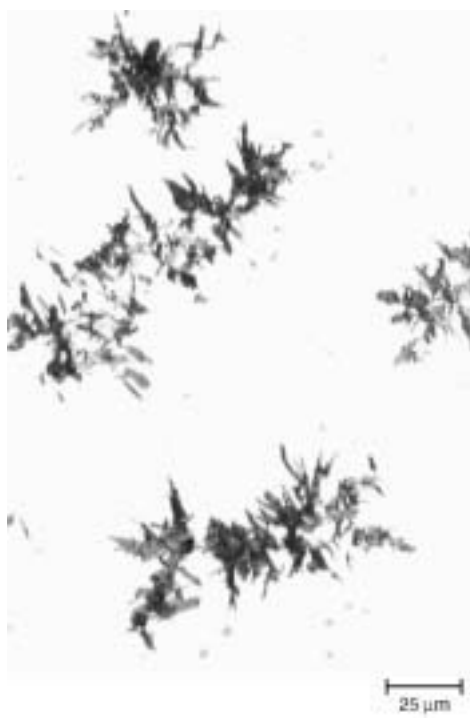


**Fig. 7** Same as in Fig. 6 but after final polishing with the 1  $\mu\text{m}$  diamond paste applied on a napless cloth. Graphite is free of any visible pullouts. As-polished. 400 $\times$

sectioned by flame cutting, the specimen must be removed well away from the heat-affected zone. The pieces cut out for metallographic examination may be ground prior to mounting (this may be done to round off sharp cut edges or to reduce the roughness of band-saw-cut surfaces) and subsequent preparation. Overheating is avoided by proper selection of the speed of cutoff saws, the use of the correct wheel, and adequate water cooling. Overheating during grinding is avoided by using fresh abrasive paper and proper cooling. When metallographic specimens are cut out from the standard cast bars, they are sometimes prepared using standard machine shop equipment, such as turning in a lathe or milling. These devices can deform the testpiece surfaces to a considerable depth, so care must be exercised to remove any damage from these operations before starting specimen preparation.

**Mounting.** Specimens can be mounted in a polymeric material using either cold or hot mounting procedures. The mounting resin is chosen depending on the cast iron hardness (soft or hard) and the need to enhance edge retention. Use of an incorrect resin, or ignoring the mounting process, can make it very difficult to obtain properly polished graphite in the area close to the specimen edge. Figures 1 and 2 show the microstructure of spheroidal graphite in ductile iron close to the edge of the specimens, which were cut off from a 30 mm (1.2 in.) diameter bar and polished with and without embedding in a polymer resin, respectively. In the specimen prepared without embedding in a resin, the graphite was pulled out, while in the specimen that was embedded in a resin and prepared, the graphite

nodules were perfectly retained. Figures 3 and 4 show that the uniform grinding of nonmounted specimens is more difficult, and the flake graphite in gray iron close to the edge of such a specimen is not polished perfectly, in comparison to well-polished graphite in the mounted specimen.

**Grinding and Polishing.** To ensure proper graphite retention, the use of an automated grinding-polishing machine is recommended over manual preparation. The automated equipment makes it possible, in comparison to manual specimen preparation, to properly control the orientation of the specimen surface relative to the grinding or polishing surface, to maintain constantly the desired load on the specimens, to uniformly rotate the specimens relative to the work surface, and to control the time for each preparation step. Proper control of these factors influences graphite retention, although other factors are also important.

A good, general principle is to minimize the number of grinding and polishing stages. Also, the load on each specimen, or on all specimens in the holder, must be chosen to obtain a correctly polished surface in the shortest possible time. This precludes the risk of pulling out the graphite phase and ensures that the graphite precipitates will be perfectly flat with sharp boundaries.

The recommended procedure for automated preparation of the specimens of nonalloyed and low-alloyed cast iron with graphite specimens is to grind with a high-quality, waterproof 220- or 240-grit (or equivalent) SiC paper until plane, with a load of 100 N for six specimens mounted in the sample holder, with central loading. Pol-

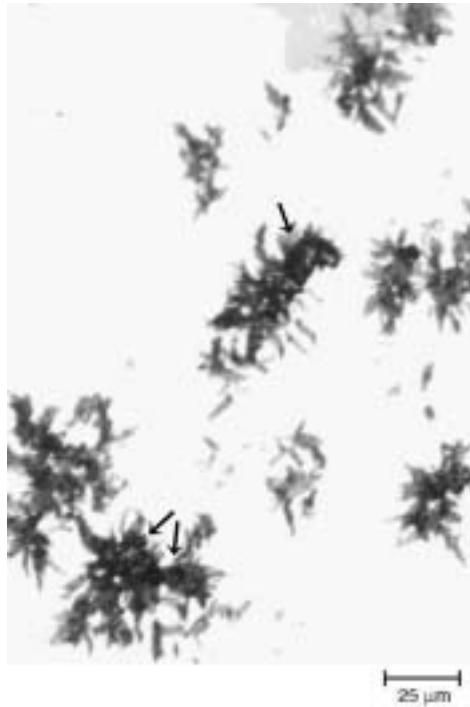


**Fig. 8** Same as in Fig. 7 but after final polishing with the 1  $\mu\text{m}$  diamond suspension applied on a napped cloth. The arrows show the pulled-out graphite. As-polished. 400 $\times$

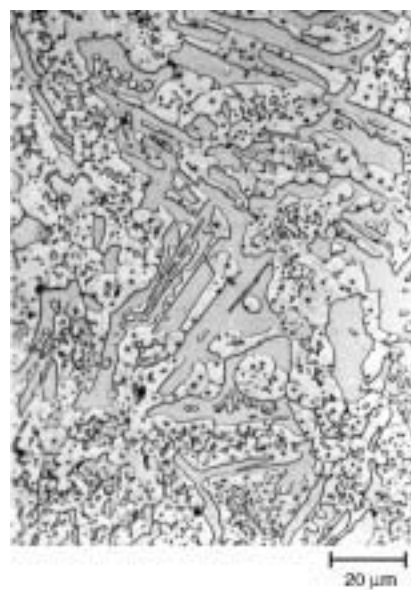


**Fig. 9** White high-chromium iron (Fe-3.2% C-4.65% Cr-2.9% Mn-0.51% Si-0.050% P-0.024% S). Eutectic and secondary carbides in the matrix. Specimen was prepared correctly. The casting was austenitized at 1000 °C (1830 °F), held 1 h, furnace cooled to 400 °C (750 °F) for 2 h, taken to salt bath at 400 °C (750 °F), held for 4 h, and air cooled. Etched with glyceregia. 500 $\times$

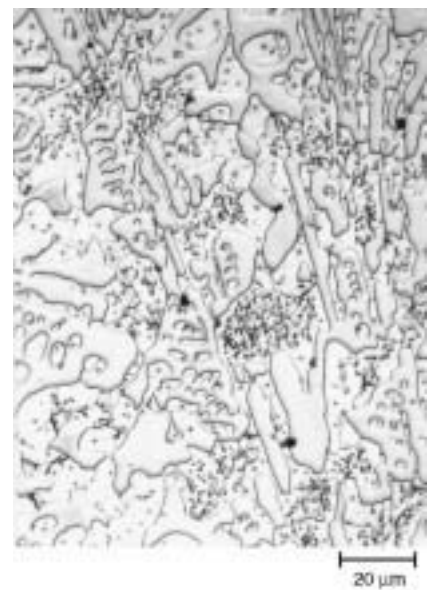


**Fig. 10** White high-chromium iron (Fe-3.16% C-8.86% Cr-0.50% Si-3.04% Mn-0.051% P-0.018% S). Eutectic and secondary carbides in the matrix. Specimen was prepared incorrectly. The casting was austenitized at 1000 °C (1830 °F), held 1 h, furnace cooled to 700 °C (1290 °F) for 2 h, taken to salt bath at 700 °C (1290 °F), held 4 h, and air cooled. Etched with glyceregia. 500 $\times$

ishing is carried out in four steps with a different grain size diamond paste:

Step	Diamond paste grain size, $\mu\text{m}$	Load, N	Duration	Recommended polishing cloth
1	9	120(a)	5 min(d)	Napless woven
2	3	120(a)	3 min(d)	Napless woven
3	1	120(a)	2 min(d)	Napless woven
4	(b)	25(c)	45–60 s(e)	Napless synthetic polyurethane

(a) Load per six specimens. (b) Aqueous 0.05  $\mu\text{m}$  alumina suspension.  
(c) Load per single specimen (switching to individual force to make specimen cleaning easier). (d) Comp direction. (e) Contra

Figure 5 shows temper graphite in malleable iron after the last step of grinding, which was carried out in three steps using, consecutively, SiC grit papers P220, P500, and P1000. Figure 6 shows the same specimen after grinding on

P220 SiC paper and then polishing with 9  $\mu\text{m}$  diamond paste according to the procedure given previously. In both cases, there is some pulled-out graphite after these steps. Each specimen was prepared further. The specimen ground with three SiC steps was polished with 3  $\mu\text{m}$  diamond suspension on a napless cloth and then with 1  $\mu\text{m}$  diamond suspension on a napped cloth. The pulled-out graphite was still visible. However, the specimen ground with P220 SiC and polished with 9  $\mu\text{m}$  diamond paste, when finished with the recommended practice given previously, was free of any visible pullouts, as shown in Fig. 7. By using a napped cloth and an aqueous 1  $\mu\text{m}$  diamond suspension for the final diamond polishing step, it was impossible to obtain perfectly retained graphite, as shown in Fig. 8. Napped cloths should not be used with diamond abrasive, either in paste, suspension, or aerosol form. Graphite retention appears to be slightly

better using diamond paste and the preferred lubricant than with an aqueous suspension, although more work needs to be conducted to determine if this difference is important. Final polishing with an alumina suspension, such as Masterprep alumina (Buehler, Ltd.), makes the graphite boundaries sharper by removing the matrix, which was smeared over the edge of the graphite during grinding and was not removed by the diamond polishing steps.

Alloyed chromium iron is much harder, and a different preparation procedure must be used. The grinding process is carried out in three steps, and polishing is carried out in three steps, although only two polishing steps are needed for most routine work. Grinding of the specimens, mounted in the sample holder, used central loading (150 N/six specimens), with high-quality SiC waterproof paper (water cooled) with the following grit sizes:

**Table 2 Etchants**

No. of etchant	Name of etchant	Composition	Comments	Ref
1	Nital	96–98 mL ethanol 2–4 mL nitric acid ( $\text{HNO}_3$ )	Most common etchant for iron, carbon, alloyed steels, and cast iron. Reveals alpha grain boundaries and constituents. The 2 or 4% solution is commonly used. Use by immersion of sample for up to 60 s.	4, p 648
2	Picral	4 g picric acid ( $(\text{NO}_2)_3\text{C}_6\text{H}_2\text{OH}$ ) 100 mL ethanol	Recommended for structures consisting of ferrite and carbides. Does not reveal ferrite grain boundaries and martensite as-quenched. Addition of approximately 0.5–1% zephirane chloride improves etch rate and uniformity.	4, p 648
3	Glyceregia (modified)	3 parts glycerine 2 parts hydrochloric acid (HCl) 1 part nitric acid ( $\text{HNO}_3$ )	For austenitic stainless steels and cast irons. Reveals grain structure; outlines sigma and carbides. Mix fresh; do not store. Use by swabbing. Heat up to 50 °C (120 °F) when etching time at 20 °C (70 °F) does not bring results.	4, p 634
4	Alkaline sodium picrate (ASP)	2 g picric acid ( $(\text{NO}_2)_3\text{C}_6\text{H}_2\text{OH}$ ) 25 g sodium hydroxide (NaOH) 100 mL distilled water	Immerse sample in solution at 60–70 °C (140–160 °F) for 1–3 min. Colors cementite ( $\text{Fe}_3\text{C}$ ) dark brown to black, depending on etching time.	4, p 646
5	Klemm I	50 mL sat. aq. sodium thiosulfate ( $\text{Na}_2\text{S}_2\text{O}_3 \cdot 5\text{H}_2\text{O}$ ) 1 g potassium metabisulfite ( $\text{K}_2\text{S}_2\text{O}_5$ )	Immerse sample for 40–100 s. Reveals phosphorus segregation (white); colors ferrite blue or red; martensite brown; cementite and austenite are unaffected	4, p 642
6	Beraha CdS	240 g aq. sodium thiosulfate ( $\text{Na}_2\text{S}_2\text{O}_3 \cdot 5\text{H}_2\text{O}$ ) 30 g citric acid ( $\text{C}_6\text{H}_8\text{O}_7 \cdot \text{H}_2\text{O}$ ) 20–25 g cadmium chloride ( $\text{CdCl}_2 \cdot 2.5\text{H}_2\text{O}$ ) 100 mL distilled water	Tint etch for iron, steel, cast irons, and ferritic and martensitic stainless steel. Dissolve in order shown. Allow each to dissolve before adding next. Allow to age 24 h at 20 °C (70 °F) in a dark bottle. Before use, filter 100 mL of solution to remove precipitates. Preetch with a general-purpose reagent. Etch 20–90 s; good for 4 h. For steels and cast irons, after 20–40 s only ferrite is colored, red or violet. Longer times color all constituents: ferrite is colored yellow or light blue; phosphide, brown; carbide, violet or blue. For stainless steels, immerse sample 60–90 s; carbides are colored red or violet-blue; matrix, yellow; colors of ferrite vary. Sulfides red-brown after 90 s	4, p 644
7	...	28 g sodium hydroxide (NaOH) 4 g picric acid ( $(\text{NO}_2)_3\text{C}_6\text{H}_2\text{OH}$ ) 1 g potassium metabisulfite ( $\text{K}_2\text{S}_2\text{O}_5$ ) 100 mL distilled water	Immerse sample in hot solution (close to boiling temperature) for 30–60 min. This reagent reveals silicon segregation in ductile iron. The colors of microstructure change themselves from green through red, yellow, blue, and dark brown to light brown as the silicon content is reduced from the graphite nodule to cell boundaries. The regions with lowest silicon content at the cell boundaries remain colorless. Before etching, ferritization of the specimen is recommended to enhance the visibility of the colors.	6
8	Murakami reagent	10 g potassium ferricyanide ( $\text{K}_3\text{Fe}(\text{CN})_6$ ) 10 g potassium hydroxide (KOH) or sodium hydroxide (NaOH) 100 mL distilled water	Use fresh, cold or hot. Cold, at 20 °C (70 °F) for up to 1.5 min, tints chromium carbides; $\text{Fe}_3\text{C}$ unattacked or barely attacked. Hot, at 50 °C (120 °F) for 3 min, tints iron phosphide. The higher temperature or etching time also tints cementite into yellow color.	4, p 646
9	Beraha reagent with selenic acid	2 mL hydrochloric acid (HCl) 0.5 mL selenic acid ( $\text{H}_2\text{SeO}_4$ ) 100 mL ethanol	For differentiation of the constituents in steadite in cast iron, immerse sample for 7–10 min; iron phosphide colored blue or green, cementite colored red, and ferrite is bright (unaffected). Preetching with nital is recommended.	4, p 643
10	Beraha-Martensite (B-M)	2 g ammonium bifluoride ( $\text{NH}_4\text{F}\cdot\text{HF}$ ) 2 g potassium metabisulfite ( $\text{K}_2\text{S}_2\text{O}_5$ ) 100 mL stock solution: 1:5, HCl to distilled water	Immerse sample for 1–3 s. Coarse martensite is blue or yellow; fine martensite and bainite are brown. Use fresh reagent, and wet sample with tap water before etching.	6, p 26
11	10% sodium metabisulfite (SMB)(b)	10 g sodium pyrosulfite ( $\text{Na}_2\text{S}_2\text{O}_5$ ) 100 mL distilled water	Tints as-quenched martensite into brown; bainite into blue; carbides, phosphides, and residual austenite, unaffected. Immerse sample in etchant solution approximately 20 s. Preetching sample with nital is recommended.	4, p 642
12	Lichtenegger and Bloech I (LB I)	20 g ammonium bifluoride ( $\text{NH}_4\text{F}\cdot\text{HF}$ ) 0.5 g potassium metabisulfite ( $\text{K}_2\text{S}_2\text{O}_5$ ) 100 mL hot distilled water	Dissolve in given order. In austenitic Cr-Ni alloys, it tints austenite and reveals dendritic segregation. Ferrite and carbides remain unaffected. Wet-etch for 1–5 min immediately after polishing.	7, p 51
13	...	50% aq. hydrochloric acid (HCl)	Immerse sample for 30–90 min. Every 15–20 min, wash sample with distilled water, quickly etch in hydrofluoric acid (conc.), and wash in tap water. When the etching process is finished, immerse sample in 5% aq. KOH or NaOH for 10–20 min, wash with distilled water in an ultrasonic washer, then in ethanol, and dry with blowing hot air.	8, p 97

(a) Potassium metabisulfite and potassium pyrosulfite are both synonymous with  $\text{K}_2\text{S}_2\text{O}_5$ . (b) Sodium metabisulfite and sodium pyrosulfite are synonymous with  $\text{Na}_2\text{S}_2\text{O}_5$ .

- First step: P220 grit until plane.
- Second step: P500 grit for 3 min.
- Third step: P1000 grit for 3 min

Polishing is done in three steps, with different grain size diamond in paste for the first two steps:

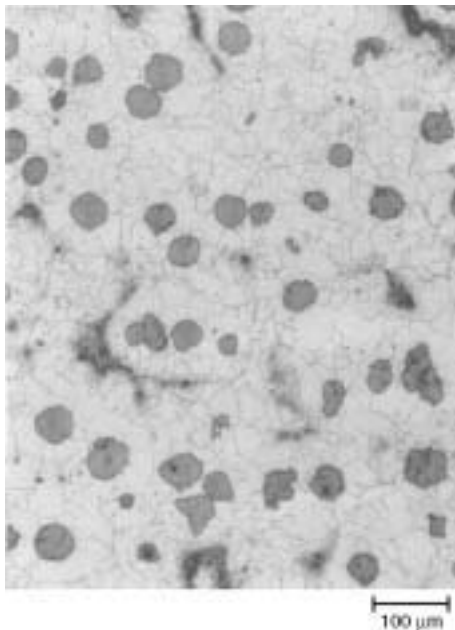


**Fig. 11** Ductile iron (Fe-3.8%C-2.4%Si-0.28%Mn-1.0%Ni-0.05%Mg) after annealing. Ferrite and approximately 5% pearlite. Etched with 2% nital. 100 $\times$ . Courtesy of G.F. Vander Voort, Buehler Ltd.

- First step: 3 μm diamond, 120 N load/six specimens for 3 min with a napless cloth.
- Second step: 1 μm diamond, 100 N load/six specimens for 3 min with a napless cloth

The last polishing step is carried out with a colloidal silica suspension on a napless synthetic

polyurethane pad but in a single specimen holder with an individual load of 30 N for 1.5 min.

Figure 9 shows the microstructure of a heat treated chromium iron after this preparation. The carbides are perfectly flat, with very sharp edges and boundaries etched uniformly. Figure 10 shows the primary eutectic carbides in the microstructure of a high-chromium iron. They appear to be sticking out from the matrix, and their boundaries are not outlined uniformly. This result occurs if the load is too low or the final polishing time on the silica suspension is too long. Both problems will result in too much removal of the softer matrix that was surrounding the primary carbides.

During grinding, the paper must be moistened with flowing tap water, and the specimens should be washed with water after each step. Also, during the first planning step, the sheet of paper should be changed every 1 min. Used grit paper is not effective and will introduce heat and damage, impairing specimen flatness. During polishing with diamond paste from a tube, the cloth is moistened with the recommended lubricant for the paste. If a water-based diamond suspension is applied on the cloth, the use of an additional lubricant is not required.

The speed of the grinding-polishing head was 150 rpm, and it was constant. The speed of the platen during grinding was always 300 rpm, and during polishing was always 150 rpm. After each grinding step, the specimens were washed with running tap water and dried with compressed air, while after each polishing step, they were washed with alcohol and dried with hot air from a hair dryer.

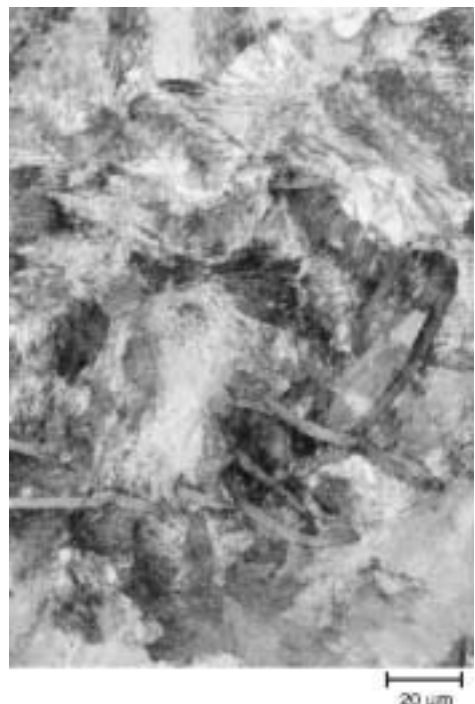


**Fig. 13** Same as in Fig. 12 but after etching with 4% picral. Pearlite was etched uniformly. 500 $\times$



**Fig. 12** As-cast gray iron (Fe-2.8%C-0.8%Si-0.4%Mn-0.1%S-0.35%P-0.3%Cr). Pearlite. Etched with 4% nital. Arrows show the white areas with weakly etched or nonetched pearlite. 500 $\times$

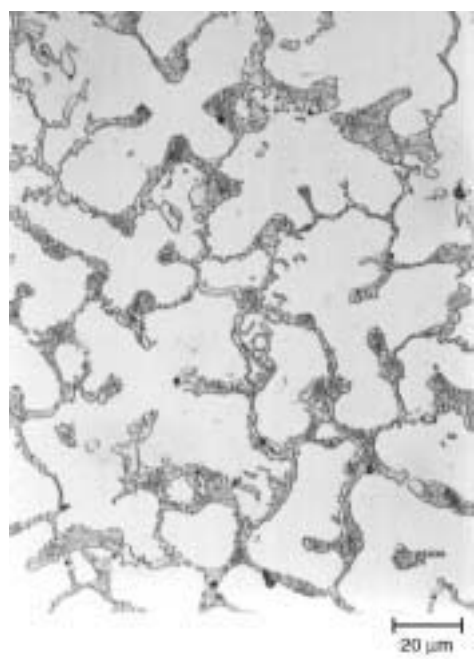


**Fig. 14** As-cast high-chromium white iron (Fe-1.57%C-18.64%Cr-2.86%Mn-0.53%Si-0.036%P-0.013%S). Eutectic chromium carbides type  $M_7C_3$  in austenitic matrix. Etched with glyceregia. 500 $\times$

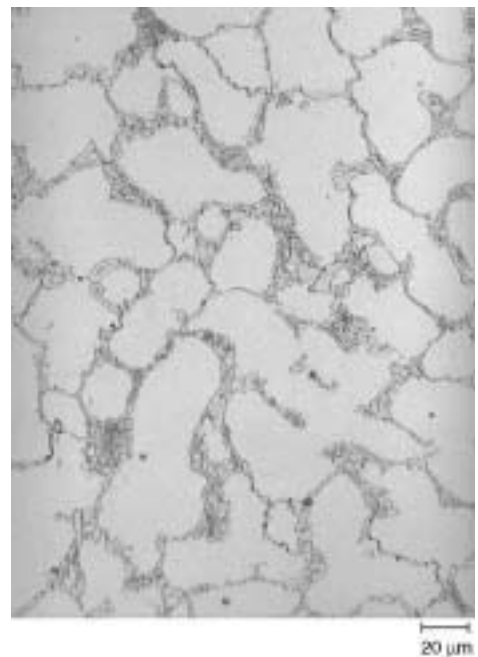


**Fig. 15** Same as in Fig. 14 but after etching with 4% nital. 500 $\times$

## Microexamination Methods

**Chemical Etching.** The examination of the iron microstructure with a light optical microscope is always the first step for phase identifi-

cation and morphology. One should always begin microstructural investigations by examining the as-polished specimen before etching. This is a necessity, of course, for cast iron specimens, if one is to properly examine the graphite phase.

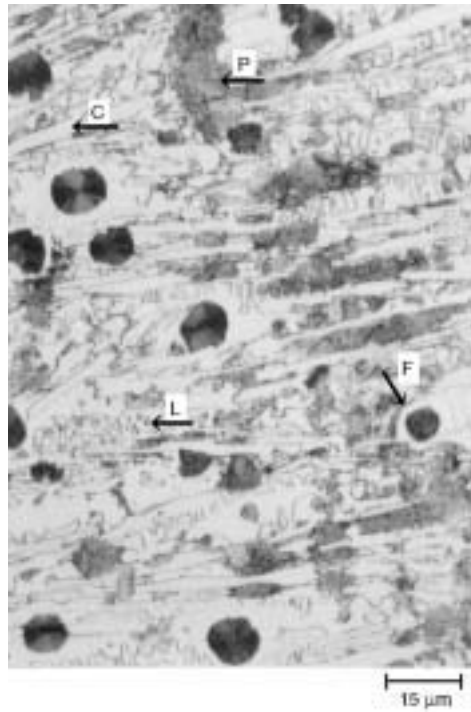


**Fig. 16** As-cast ductile iron (Fe-3.07% C-0.06% Mn-2.89% Si-0.006% P-0.015% S-0.029% Mg). C, cementite; L, ledeburite; F, ferrite; and P, pearlite. Etched with 4% nital. 650× (microscopic magnification 500×)

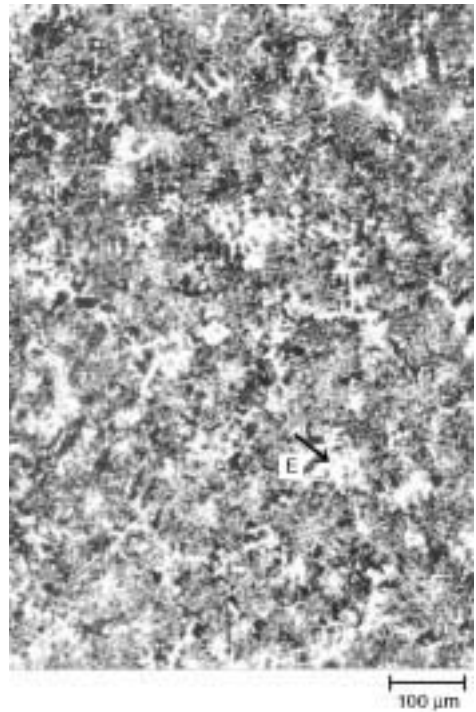


**Fig. 18** As-cast gray iron (Fe-3.24% C-2.32% Si-0.54% Mn-0.71% P-0.1% S). E, phosphorous ternary eutectic. Etched with 4% nital. 100×

**Standard Etchants.** To see the microstructural details, specimens must be etched. Etching methods based on chemical corrosive processes have been used by metallographers for many years to reveal structures for black-and-white imaging.

Specimens of nonalloyed and low-alloyed irons containing ferrite, pearlite, the phosphorus eutectic (steadiate), cementite, martensite, and bainite can be etched successfully with nital at room temperature to reveal all of these microstructural constituents. Usually, this is a 2 to 4% alcohol solution of nitric acid ( $\text{HNO}_3$ ) (Table 2, etch No. 1). Figure 11 shows a nearly ferritic annealed ductile iron with uniformly etched grain boundaries of ferrite and a small amount of pearlite. Nital is very sensitive to the crystallographic orientation of pearlite grains, so, in the case of a fully pearlitic structure, it is recommended to use picral, which is an alcohol solution of 4% picric acid (Table 2, etch No. 2). Figures 12 and 13 show the differences in revealing the microstructure of pearlite with nital or picral. Picral does not etch the ferrite grain boundaries, or as-quenched martensite, but it etches the pearlitic structure more uniformly, while nital leaves white, unetched areas, especially in the case where pearlite is very fine.

When the austempering heat treatment is very short, the microstructure of austempered ductile iron (ADI) consists of martensite and a small amount of acicular ferrite. After etching in 4% nital, martensite as well as acicular ferrite are both etched intensively, which makes it very dif-

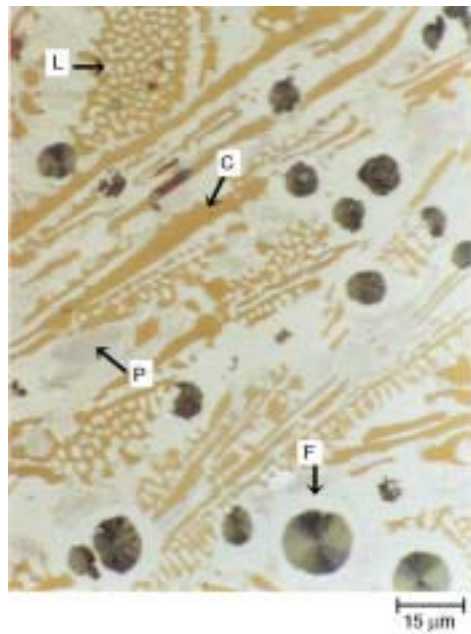


**Fig. 17** Same as in Fig. 16 but after etching with hot alkaline sodium picrate. C, eutectic cementite; L, ledeburite; F, ferrite; and P, pearlite with slightly etched cementite. 650× (microscopic magnification 500×)

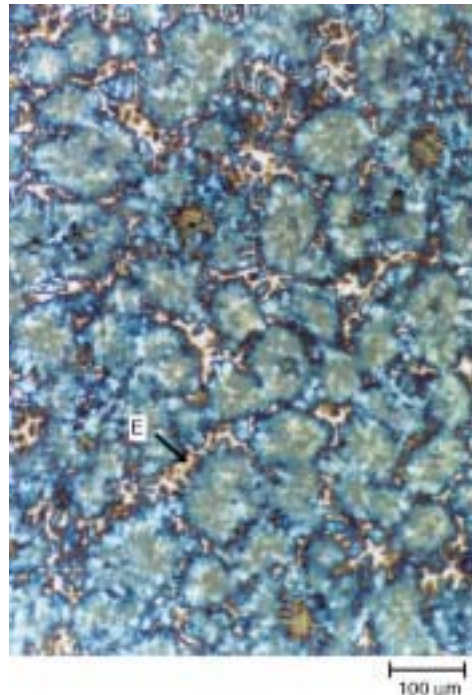


**Fig. 19** Same as in Fig. 18 but after etching with Klemm I reagent. E, phosphorous ternary eutectic. 100×

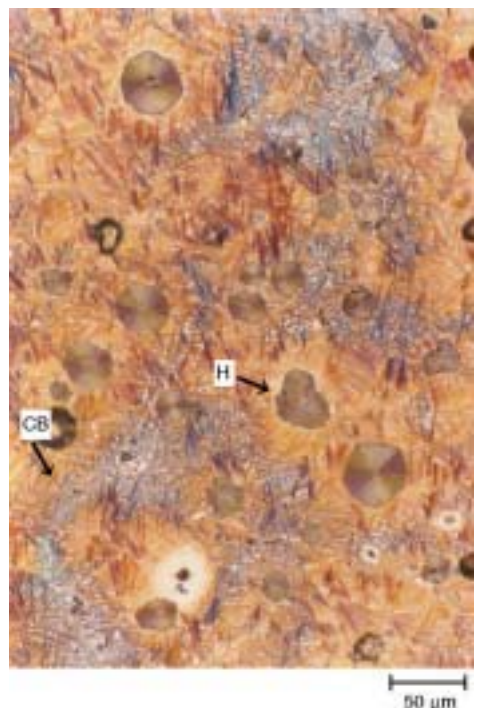


**Fig. 20** Austempered ductile iron (Fe-3.6% C-2.5% Si-0.06% P-1.5% Ni-0.7% Cu). CB, cell boundaries; H, ferritic halo around the graphite nodules. Etched with Klemm I reagent. 200×

ficult to distinctly see the needles of acicular ferrite. Picral reveals this phase very well; martensite is barely etched due to the very short austempering heat treatment of the specimen,

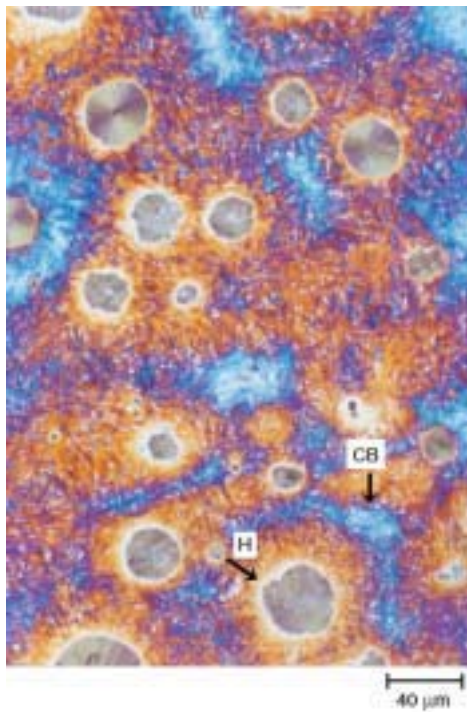


**Fig. 21** Same as in Fig. 20 but after etching with Beraha's CdS reagent. H, ferritic halo; CB, cell boundaries. 250 $\times$

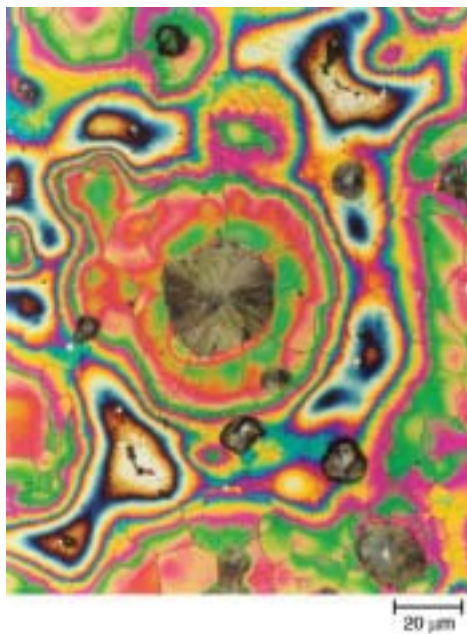


**Fig. 22** Nodular iron (Fe-3.9% C-2.9% Si-0.32% Mn-0.06% P-0.037% Mg-1.5% Ni-0.57% Cu). Silicon microsegregation was revealed. The casting was annealed. Etched with hot aqueous solution of sodium hydroxide, picric acid, and potassium pyrosulfite (Table 2, etchant No. 7). 500 $\times$

which was 2 min, because the martensite was as-quenched. The needles of acicular ferrite are dark and very sharp (Fig. 32, 33). In this case, picral is very convenient for estimating the amount and morphology of the acicular ferrite in the ADI microstructure. Picral is safer to be

stored in the lab than nital, which can be an explosive mixture under certain conditions when it is stored in a tightly closed bottle.

Glyceregia (Table 2, etch No. 3), which is a mixture of glycerine, hydrochloric acid (HCl), and nitric acid ( $HNO_3$ ), is recommended for revealing the microstructure of high-chromium and chromium-nickel-molybdenum irons. Figure 14 shows the microstructure of a high-chromium cast iron after etching with glyceregia (see also Fig. 43, 49, and 96). Nital can be also used for revealing the carbide morphology in the microstructure of chromium or chromium-nickel irons when the carbon and chromium content promotes solidification of eutectic carbides. When the microstructure of a high-chromium white iron contains columnar primary carbides, glyceregia is recommended.

Figure 15 shows the microstructure of the same cast iron as Fig. 14 but after etching with 4% nital (see also Fig. 40, 41). Both etchants reveal carbide boundaries sharply and uniformly.

**Selective Color Etching.** If the black-and-white etchants are inadequate for positive identification of the iron microstructures, other procedures must be used, such as selective color etching. The reagents referred to as tint etchants are usually acidic solutions with either water or alcohol as a solvent. They are chemically balanced to deposit a thin (40 to 500 nm), transparent film of oxide, sulfide, complex molybdate, elemental selenium, or chromate on the specimen surface. Coloration is developed by interference between light rays reflected at the in-



**Fig. 23** As-cast gray iron (Fe-3.33% C-1.64% Si-0.31% Mn-1.37% P-0.107% S). Ternary phosphorus eutectic. Etched with 4% nital. 1300 $\times$  (microscopic magnification 1000 $\times$ )



**Fig. 24** Same as in Fig. 23 but after etching with hot alkaline sodium picrate. C, cementite; F, ferrite (unaffected); IP, iron phosphide + ferrite; and TiN, titanium nitride. 1300 $\times$  (microscopic magnification 1000 $\times$ )

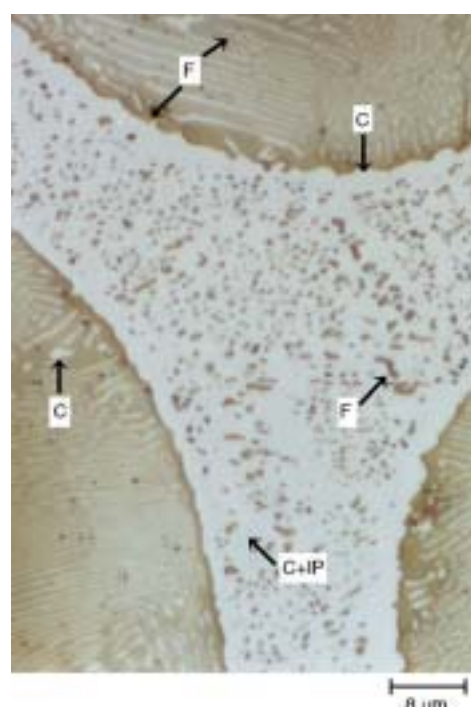


**Fig. 25** Same as in Fig. 23 but after etching with Klemm I reagent. F, ferrite; C, cementite; and C + IP, cementite + iron phosphide inside the precipitate of phosphorous eutectic. 1300 $\times$  (microscopic magnification 1000 $\times$ )

ner and outer film surfaces. Crystallographic orientation, local chemical composition, and etching time affect film thickness and control color production. The use of selective etchants

is invaluable for quantitative metallography, a field of growing importance (Ref 5).

When ferritic-pearlitic microstructures of cast iron contain large amounts of cementite and led-

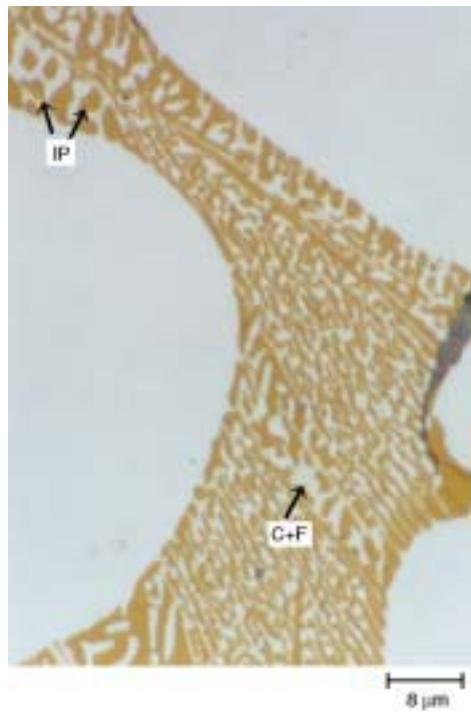


**Fig. 26** Same as in Fig. 23 but after etching with hot Murakami's reagent. IP, iron phosphide; C + F, cementite + ferrite inside the precipitate of phosphorous eutectic. 1300 $\times$  (microscopic magnification 1000 $\times$ )

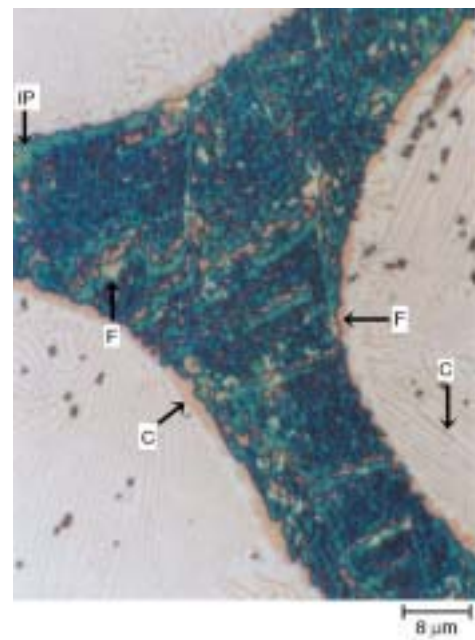


**Fig. 28** Same as in Fig. 25 but after etching with Beraha's reagent with selenic acid. IP, iron phosphide; C, cementite; and F, ferrite. The dark points in pearlite, which look like artifacts, can be iron phosphide precipitates or fine, nonmetallic inclusions. 1300 $\times$  (microscopic magnification 1000 $\times$ )

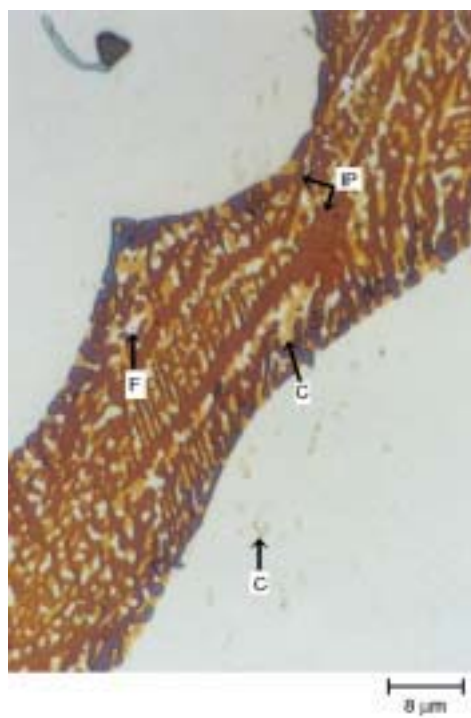


**Fig. 27** Same as in Fig. 26 but after overetching with hot Murakami's reagent. IP, iron phosphide; C, cementite; and F, ferrite. 1300 $\times$  (microscopic magnification 1000 $\times$ )

eburite, the differentiation of the white structural constituents is difficult after etching a specimen with nital. In such cases, hot alkaline sodium picrate (ASP) is recommended (Table 2, etch No. 4), which reveals cementite, tinted a brown color, while ferrite remains unaffected. This etch is a mixture of sodium hydroxide (NaOH), picric acid, and distilled water. Figure 16 shows the microstructure of a thin-walled, chilled ductile iron casting after etching with nital, while Fig. 17 shows the microstructure of the same specimen after etching with ASP; the brown-colored cementite and ledeburite are clearly visible in the pearlitic-ferritic matrix (the cementite in pearlite was also slightly tinted). It allows one to estimate the amount of cementite that should be removed from the casting microstructure in the annealing process.

Segregation of silicon and phosphorus in iron is very strong and can be revealed with selective color etching methods. Klemm's I reagent (Table 2, etch No. 5), which tints ferrite while austenite and carbides remain colorless, consists of potassium metabisulfite ( $K_2S_2O_5$ ) and a cold-saturated water solution of sodium thiosulfate ( $Na_2S_2O_3 \cdot 5H_2O$ ) and is one of the etchants that can be used to reveal phosphorus and silicon segregation.

Usually, the distribution of the phosphorus eutectic, which solidifies in gray iron on the cell boundaries, is revealed by etching up to 4 min in 4% nital. Figure 18 shows the microstructure of as-cast gray iron with the ternary phosphorous eutectic. The cell boundaries, filled with steatite,



**Fig. 29** As-cast gray iron (Fe-3.62%C-2.03%Si-1.13%P-0.61%Mn-0.137%S-0.113%Cr-0.478%Ni-0.004%Al). E, binary phosphorous eutectic; F, ferrite at the graphite precipitate; and P, pearlite. Etched with 4% nital. 500 $\times$



**Fig. 30** Same as in Fig. 29 but after etching with hot alkaline sodium picrate and 4% nital. Pearlitic matrix is revealed; phosphorous eutectic is unaffected. 500 $\times$

are white, while their interiors are almost black due to overetching the pearlitic-ferritic matrix. Figure 19 shows the same microstructure after etching with Klemm's I reagent. The microregions inside the eutectic cells with a lower phosphorus content are tinted a blue color, while the



**Fig. 31** Same as in Fig. 29 but after etching with hot Murakami reagent. Only brown-tinted iron phosphide was revealed. 500 $\times$

areas with the ternary eutectic, situated at the boundaries of the eutectic cells, are almost colorless. In both cases, the cementite and iron

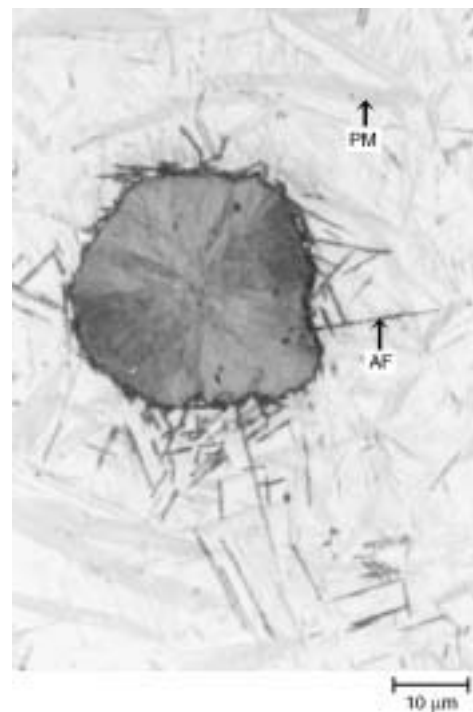


**Fig. 33** Same as in Fig. 32 but after etching with 4% picral. AF, acicular ferrite; PM, plate martensite. 1000 $\times$

phosphide in steadite are not etched, and the network is clearly visible.

Figure 20 shows silicon segregation in an ADI microstructure after etching with Klemm's I reagent. The regions outlining the cell boundaries, low in silicon, are tinted a blue color, while the very thin halos around the graphite nodules, where the silicon content is highest, remain colorless. Acicular ferrite is orange, and austenite is not tinted. Figure 21 shows the same microstructure after etching with Beraha's Cds reagent (Table 2, etch No. 6), an aqueous solution of sodium thiosulfate ( $\text{Na}_2\text{S}_2\text{O}_3 \cdot 5\text{H}_2\text{O}$ ), citric acid ( $\text{C}_6\text{H}_8\text{O}_7 \cdot \text{H}_2\text{O}$ ), and cadmium chloride ( $\text{CdCl}_2 \cdot 2.5\text{H}_2\text{O}$ ). The silicon segregation is revealed the same way as after using Klemm's I reagent.

To reveal silicon segregation in nonalloyed ductile cast iron inside eutectic cells, the hot aqueous solution of sodium hydroxide, picric acid, and potassium pyrosulfite ( $\text{K}_2\text{S}_2\text{O}_5$ ) can be used (Table 2, etch No. 7). Figure 22 shows the different colors of the microstructure, which change from green through red, yellow, blue, and dark brown to light brown as the silicon content is changing from the graphite nodule to the cell boundaries. The regions with the lowest silicon content at the cell boundaries remain colorless. Before etching, ferritization of the specimen was carried out to enhance the visibility of the microstructural colors.

The revealing and differentiation of all constituents in steadite is invaluable for the determination of the type of eutectic as well as the

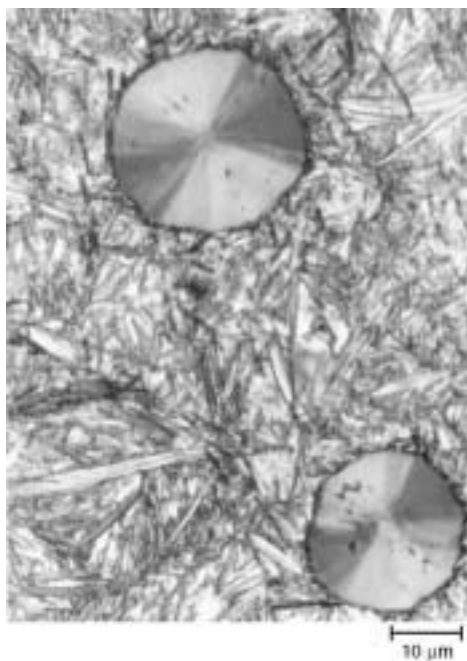


**Fig. 32** Austempered ductile iron (Fe-3.6%C-2.5%Si-0.056%P-0.052%Mg-0.7%Cu). Martensite and acicular ferrite. The casting was austempered at 900 °C (1650 °F), held 2 h, taken to salt bath at 360 °C (680 °F), held 2 min, and air cooled. Etched with 4% nital. 1000 $\times$

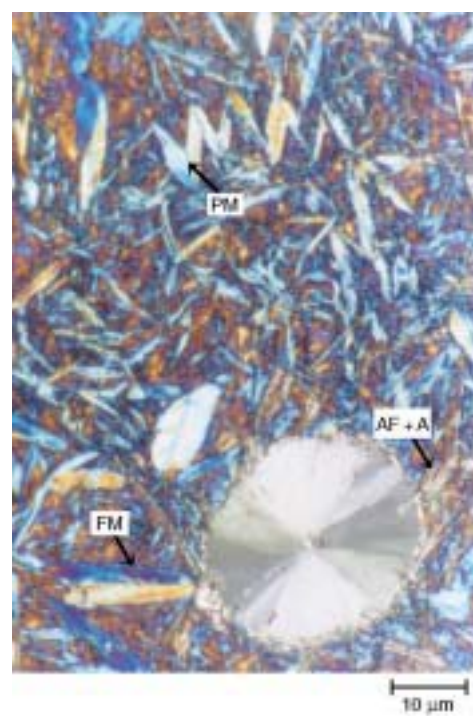


**Fig. 34** Same as in Fig. 32 but after etching with Beraha-Martensite reagent. PM, blue-yellow plate martensite; FM, brown fine martensite; and AF + A, dark needles of acicular ferrite surrounded with colorless austenite. 1000 $\times$



**Fig. 35** Same as in Fig. 32 but after etching with 10% sodium metabisulfite. PM, plate martensite; FM, fine martensite; and AF + A, acicular ferrite and austenite. 1000 $\times$

amount of each constituent. In the case of the ternary phosphorous eutectic, which consists of ferrite, cementite, and iron phosphide ( $\text{Fe}_3\text{P}$ ), nital does not help in the identification of the con-

stituents, nor does it provide enough information about distribution of the eutectic constituents. Figure 23 shows the microstructure of the ternary phosphorous eutectic in gray iron after etch-

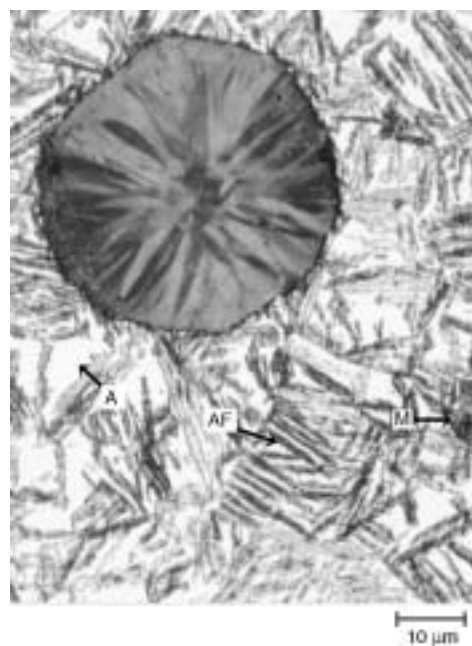


**Fig. 36** Austempered ductile iron (Fe-3.6% C-2.5% Si-0.052% Mg-0.7% Cu). AF, acicular ferrite; A, austenite; and M, martensite. The casting was austempered at 900 °C (1650 °F), held 2 h, taken to salt bath at 360 °C (680 °F), held 30 min, and air cooled. Etched with 4% nital. 1000 $\times$

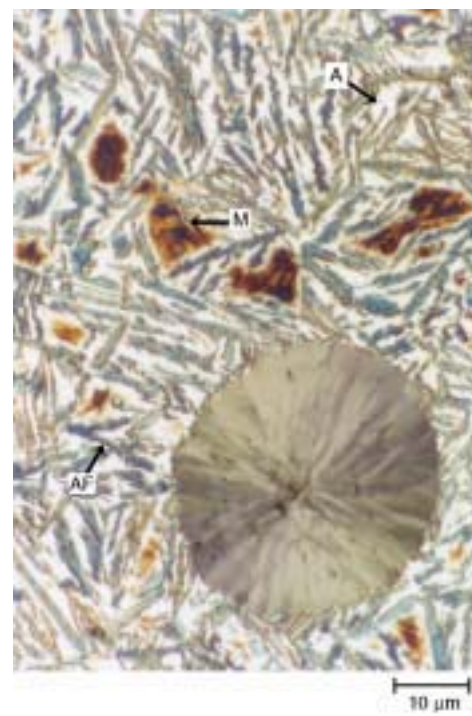


**Fig. 38** Same as in Fig. 36 but after etching with 10% sodium metabisulfite. AF, acicular ferrite; A, austenite; and M, martensite. 1000 $\times$

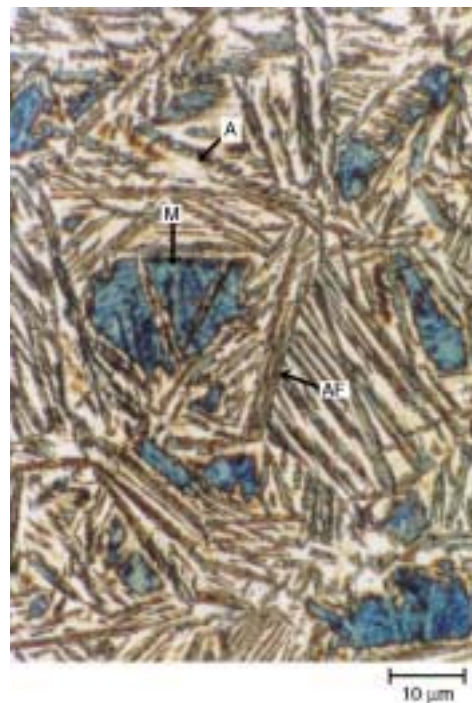


**Fig. 37** Same as in Fig. 36 but after etching with Beraha-Martensite reagent. AF, acicular ferrite; A, austenite; and M, martensite. 1000 $\times$

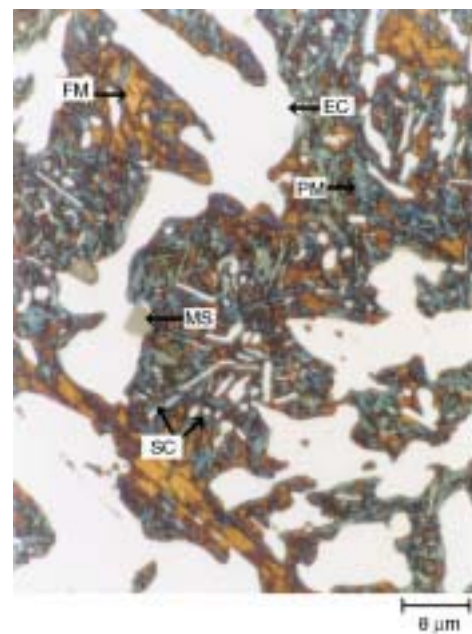


**Fig. 39** White alloyed cast iron (Fe-3.4% C-0.92% Mn-1.89% Si-9.52% Cr-6.27% Ni). Etched with Beraha-Martensite. PM, plate martensite; FM, fine martensite; EC, eutectic carbides type  $\text{M}_7\text{C}_3$ ; SC, secondary carbides; and MS, manganese sulfite. The casting was heat treated: austenitized at 750 °C (1380 °F), held 2 h, and air cooled; tempered at 250 °C (480 °F), held 4 h, and air cooled. 1300 $\times$  (microscopic magnification 1000 $\times$ )

ing in 4% nital. The white areas that surround the ternary eutectic and are also visible inside the eutectic can be either ferrite or cementite. Figure 24 shows the microstructure of the same specimen after selective color etching with hot ASP (Table 2, etchant No. 4). Cementite in the eutectic is tinted brown and blue colors (also in pearlite), while ferrite and iron phosphide are not tinted. To reveal the ferrite, the same specimen was etched with Klemm's I reagent. Figure 25 shows the eutectic regions with precipitates of brown ferrite (also in pearlite), while cementite and iron phosphide are not tinted.

Murakami's reagent (Table 2, etch No. 8), used at 50 °C (120 °F) for 3 min and containing potassium hydroxide (KOH), potassium ferrocyanide ( $\text{K}_3\text{Fe}(\text{CN})_6$ ), and distilled water, can be used for revealing and estimating the amount of iron phosphide in steadite. Figure 26 shows this constituent of the ternary phosphorous eutectic microstructure, which was tinted a light-brown color, while cementite and ferrite remained colorless. The microstructure of the same specimen after overetching (5 min) with the same reagent is shown in Fig. 27. This time, cementite was also revealed and was tinted a yellow color, while ferrite remained white. The color of the iron phosphide changed to a dark-brown and gray-blue color. Nevertheless, extending the etching time beyond 3 min is not recommended, because this can falsify the true results of the microstructural examination.

Good differentiation of all constituents in the ternary phosphorus eutectic can be obtained with Beraha's reagent (Table 2, etch No. 9), a mixture of hydrochloric acid (HCl), selenic acid

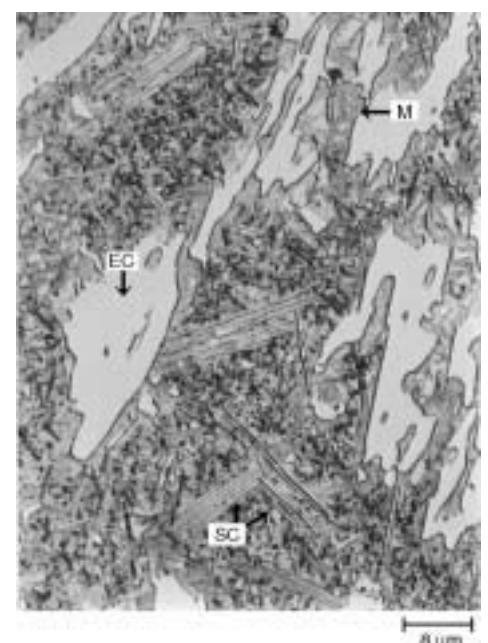


**Fig. 40** Same white iron as in Fig. 39 but after etching with 4% nital. M, martensite; EC, eutectic carbides; and SC, secondary carbides. 1300 $\times$  (microscopic magnification 1000 $\times$ )

( $H_2SeO_4$ ), and ethanol. According to Beraha, this etchant tints iron phosphide a dark-blue color, cementite a violet or dark red, and ferrite remains white. Figure 28 shows the microstruc-

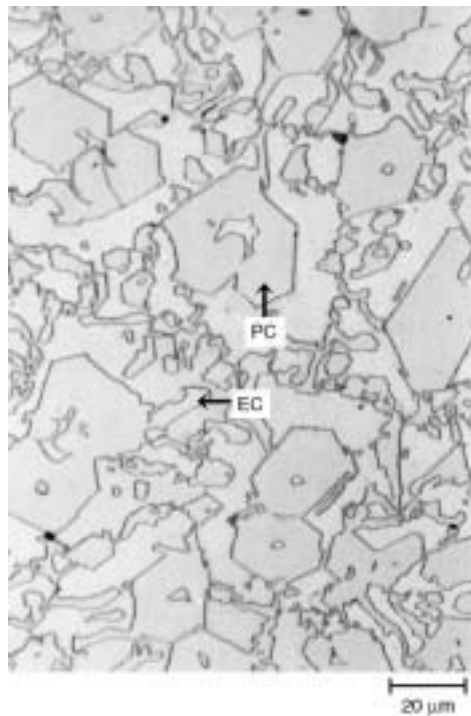


**Fig. 41** Same white iron as in Fig. 39 and 40 but as-cast. Eutectic carbides in austenitic matrix. Etched with glyceregia. 500×

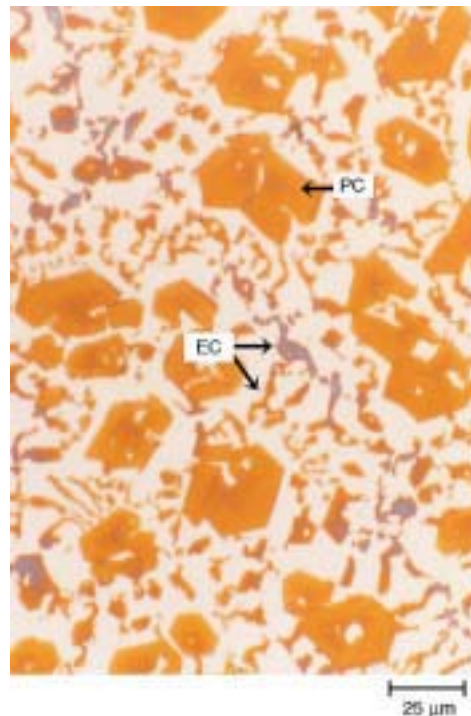


**Fig. 42** Same as in Fig. 41 but after etching with Lichtenegger and Bloech I. Austenite is dark brown, and dendritic segregation is visible around unaffected carbides. 1000×

ture of the ternary eutectic, with cementite tinted a light-pink color, while the rest of the constituents were colored properly.



**Fig. 43** As-cast high-chromium white iron ( $Fe-4.52\%C-0.4\%Si-2.86\%Mn-35.0\%Cr-0.06\%P-0.012\%S$ ). PC, primary carbides; EC, eutectic carbides, both  $M_7C_3$  type. Etched with glyceregia. 500×



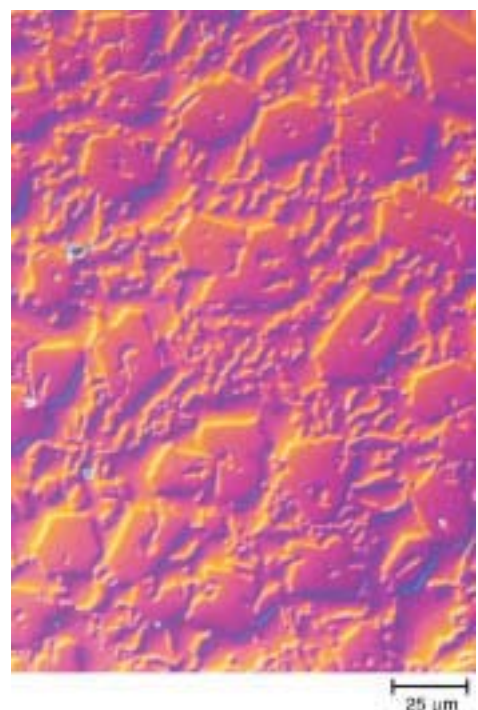
**Fig. 44** Same as in Fig. 43 but after etching with Murakami's reagent (at room temperature). PC, orange primary carbides; EC, orange and gray eutectic carbides. 400×

Figure 29 shows the microstructure of the pseudobinary phosphorous eutectic, which consists of iron phosphide and ferrite, after etching with 4% nital. The same specimen was etched with hot ASP (Table 2, etchant No. 4). This did not tint the iron phosphide or the ferrite. Because cementite is not present in the eutectic, the only etching was of cementite in the pearlite, which showed up very lightly. To reveal the microstructure of the eutectic, the specimen was next etched with 4% nital. Figure 30 shows the results after using hot ASP and then nital. Hot Murakami's reagent perfectly tinted the iron phosphide in the binary phosphorous eutectic a brown color, while pearlite was colorless, as shown in Fig. 31.

Beraha-Martensite (B-M) (Table 2, etch No. 10) and aqueous 10% sodium metabisulfite (SMB) (Table 2, etch No. 11) reagents for selective color etching are very useful in cases where microstructural details are very fine and barely visible after etching with nital. They reveal all of the constituents, tinting them to expected colors that are useful for verifying that the heat treatment process was carried out correctly.

The B-M etchant is a mixture of stock solution (1:5, HCl to water), potassium metabisulfite ( $K_2S_2O_5$ ), and ammonium acid fluoride ( $NH_4F \cdot HF$ ). According to Ref 6, B-M tints martensite a blue color and bainite a brown color, while the residual austenite and carbides remain unaffected.

The B-M etchant can be used for identification of the constituents after heat treatment of cast iron by tinting phases to different colors. It also



**Fig. 45** Same as in Fig. 43 but as-polished and examined in differential interference contrast. Primary and eutectic carbides are sticking up from the softer austenitic matrix. 400×

improves microstructural contrast, enhancing visibility and permitting estimation of even small amounts of the residual austenite (although x-ray diffraction results are always more than 10% greater than by light microscopy) and fine carbides. Figure 32 shows the black-white mi-

crostructure of ADI after etching with 4% nital, while Fig. 33 shows the same microstructure after etching with 4% picral. Figures 34 and 35

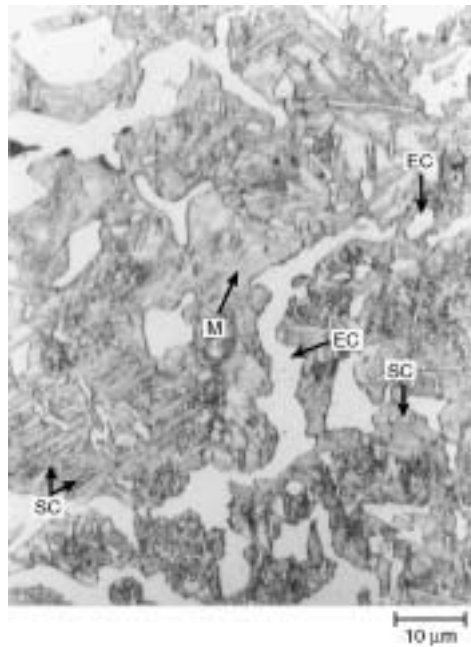


**Fig. 46** Same white iron as in Fig. 39 but after slight etching with 4% nital and examined in bright-field illumination. EC, eutectic carbides type  $M_7C_3$ ; SC, secondary carbides; and M, martensite. 1000 $\times$

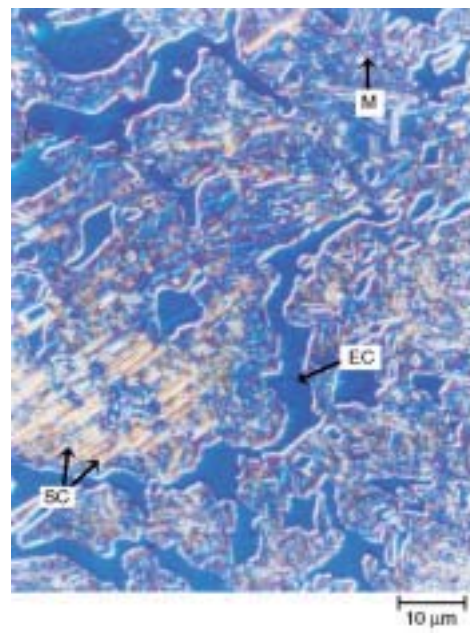


**Fig. 48** Same as Fig. 46 but examined in differential interference contrast. EC, eutectic carbides; SC, secondary carbides; and M, martensite. 1000 $\times$

show the microstructure of the same specimen after color etching, respectively, with B-M and with aqueous 10% SMB etchants. The SMB tints martensite a brown color and bainite a blue color, while austenite and carbides are colorless. Both etching time in B-M and the different crystallographic orientations affected the color of the coarse, high-carbon martensitic plates, which vary from blue to yellow. The brown areas in the microstructure (Fig. 34) are the patches of fine martensite. This color differentiation of microstructure occurs due to the change in size of the plate martensite as transformation progresses. However, this is not the only factor, because some of the larger plates are also brown. There is only a very small amount of austenite, which surrounds the acicular ferrite at the graphite nodules and in the matrix. The SMB etchant is even more useful than the B-M etchant in the case where the dominating phase in the ADI microstructure is martensite, and acicular ferrite is weakly visible. In ADI, the martensite of both types is tinted a brown color, the acicular ferrite, that is, blue color, while austenite is colorless, which was shown in Fig. 35 (see the section "Ductile Iron" in this article).

Figure 36 shows the microstructure of ADI after etching with 4% nital, while Fig. 37 and 38 show the same microstructure after etching with B-M and 10% SMB, respectively. Nital etched the acicular ferrite, while the austenite is white. Some areas that were darkened may be martensite, but there is no clear distinction between martensite and acicular ferrite with nital. Selec-

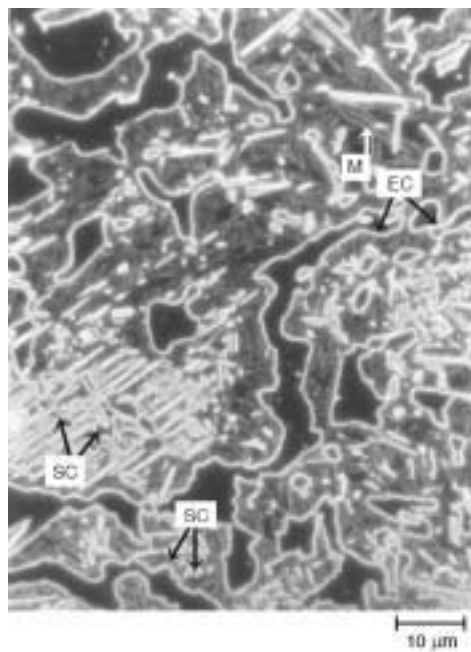


**Fig. 47** Same as in Fig. 46 but examined in dark-field illumination. EC, eutectic carbides; SC, secondary carbides; and M, martensite. 1000 $\times$

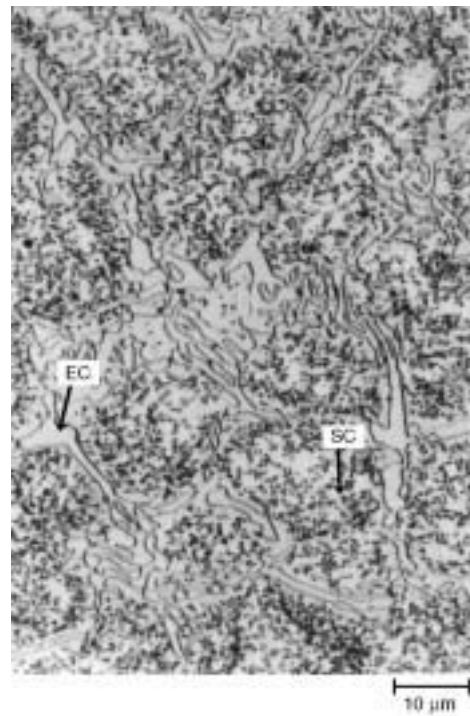


**Fig. 49** Same white iron as in Fig. 14 and 15 but casting was heat treated at 1000 °C (1830 °F), held 1 h, furnace cooled to 400 °C (750 °F) for 2 h, taken to salt bath at 400 °C (750 °F), held 4 h, and air cooled. Examined in bright-field illumination. EC, eutectic carbides type  $M_7C_3$ ; SC, secondary carbides. Etched with glyceregia. 1000 $\times$

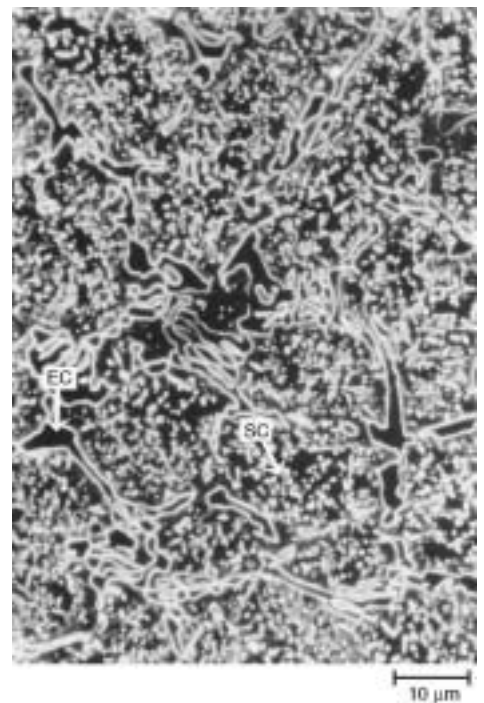


**Fig. 50** Same as in Fig. 49 but examined in dark-field illumination. EC, eutectic carbides; SC, secondary carbides. 1000 $\times$

tive color etching with the two previously mentioned reagents clearly revealed small patches of martensite, which were blue after etching with B-M and brown after etching with 10% SMB; acicular ferrite was colored blue (darker with



**Fig. 51** Graphite nodule examined in bright-field illumination. As-polished. 1000×

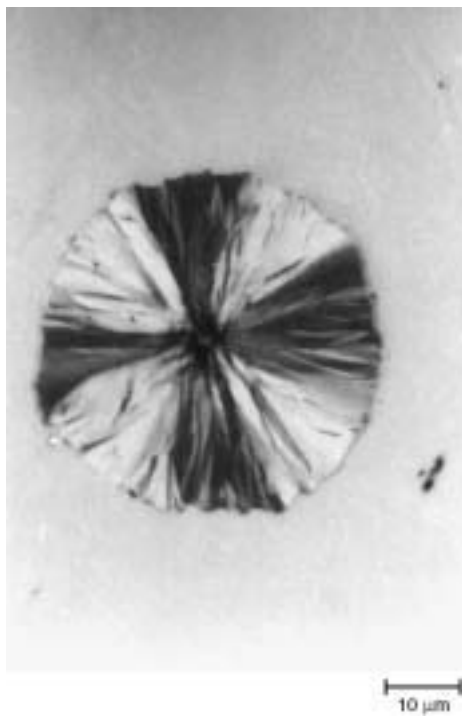


**Fig. 52** Same as in Fig. 51, but graphite nodule was examined in crossed polarized light. 1000×

B-M than with SMB), and austenite remained colorless.

The same results were achieved with the use of B-M reagent to reveal the microstructure of

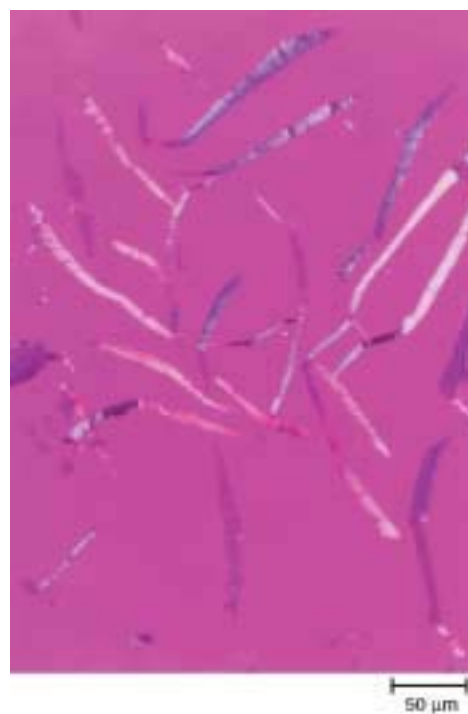


**Fig. 53** Flake graphite in as-cast gray iron examined in crossed polarized light. As-polished. 200×



**Fig. 54** Same as in Fig. 53 but microstructure was examined in crossed polarized light. Acicular ferrite is shining brightly; plate martensite is slightly gray-blue. 1000×

alloyed cast iron after heat treatment. The microstructure, which is shown in Fig. 39, consists of brown patches of fine martensite (which may have transformed from austenite during or after tempering), while the blue needles are high-carbon plate martensite. Figure 40 shows the microstructure of the same specimen after etching with 4% nital; in this case, the recognition of martensite is not straightforward.

Figures 41 and 42 show the microstructure of the same iron but in the as-cast condition after etching with glyceregia and with Lichtenegger and Bloech I (LBI), respectively (Table 2, etchant No. 3 and 12). The LBI is an aqueous solution of ammonium bifluoride ( $\text{NH}_4\text{F}\cdot\text{HF}$ ) and potassium metabisulfite ( $\text{K}_2\text{S}_2\text{O}_5$ ) (Table 2, etch No. 12). In chromium-nickel alloys, LB I tints austenite, while carbides and ferrite (if present) remain unaffected (white). Glyceregia outlines only the eutectic carbides, while the LB I etchant also reveals microsegregation. The microstructure shown in Fig. 42 consists of austenite, tinted brown and blue color, and white (noncolored) carbides. The blue austenitic areas surrounding

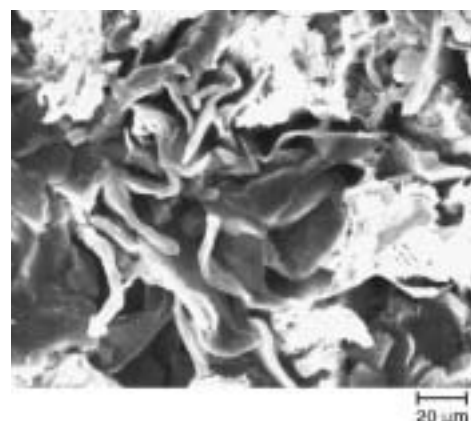


**Fig. 55** Flake graphite in as-cast gray iron examined with SEM. Sample was deeply etched with 50% HCl. 500×

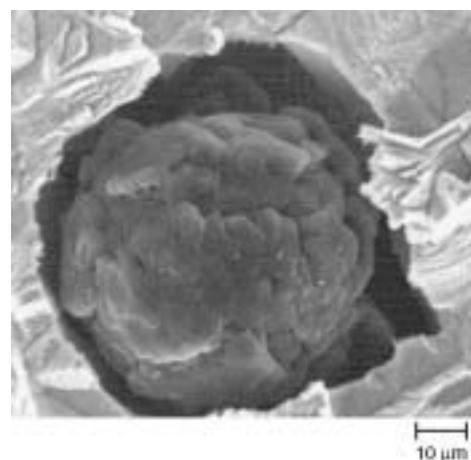


**Fig. 56** Nodular graphite in as-cast ductile iron examined with SEM. Sample was deeply etched with 50% HCl. 1000×

the eutectic carbides indicate regions with a lower concentration of carbide-forming elements, such as carbon and chromium, and perhaps a higher concentration of elements that are not present in the carbides, such as silicon and nickel.

Figure 43 shows the microstructure of a high-chromium cast iron after etching with glycerceria, revealing columnar primary carbides and eutectic carbides, both  $(\text{FeCr})_7\text{C}_3$  type, uniformly distributed in the matrix. Figure 44 shows the microstructure of the same specimen after etching with the standard Murakami's etchant at room temperature. The carbides are tinted an orange color, while the matrix is not colored. X-ray diffraction determined that the matrix was austenitic-ferritic; the matrix was not colored us-

ing the LB I tint etchant due to missing nickel in that iron.

The basic etchants mentioned previously, which are suitable for revealing microstructures

as well as for phase identification in irons, are listed in Table 2.

**Dark-Field Illumination and Differential Interference Contrast.** Dark-field illumination (DFI) technique for microstructural examination produces a very strong image contrast that makes it possible to see features in the microstructure that are invisible or weakly visible in bright-field illumination (BFI) when the surface of the specimen is normal to the optical axis of the microscope and white light is used. This image contrast is a result of reversing the image, which is bright in BFI, into a dark one when DFI is used.

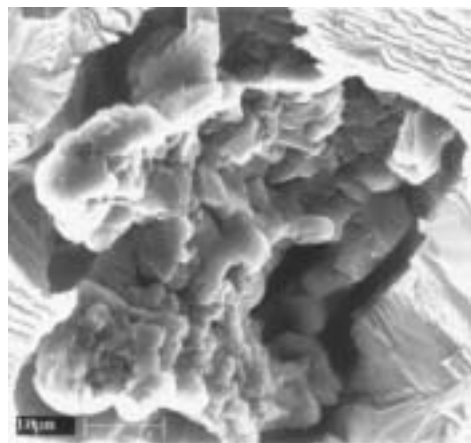


**Fig. 57** Compacted graphite examined with SEM. Sample was deeply etched with 50% HCl. 1500×



**Fig. 58** Hypoeutectic as-cast gray iron (Fe-2.8%C-1.85%Si-0.5%Mn-0.04%P-0.025%S). Flake graphite type A. As-polished. 100×

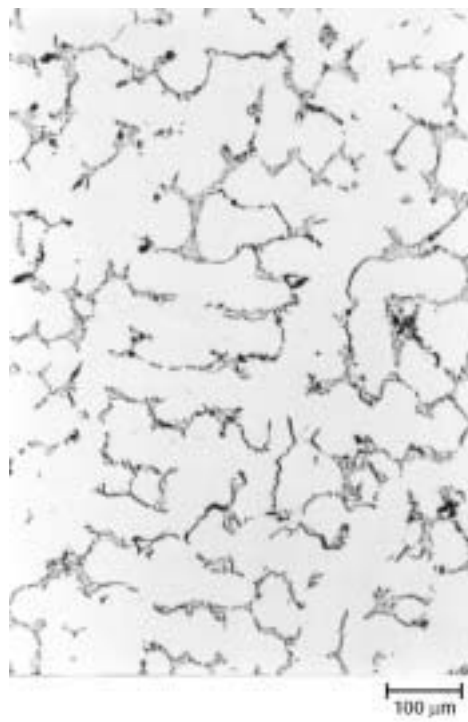


**Fig. 59** Hypoeutectic as-cast gray iron (Fe-2.1%C-2.8%Si-0.38%Mn-0.06%P-0.03%S). Flake graphite type D. As-polished. 100×

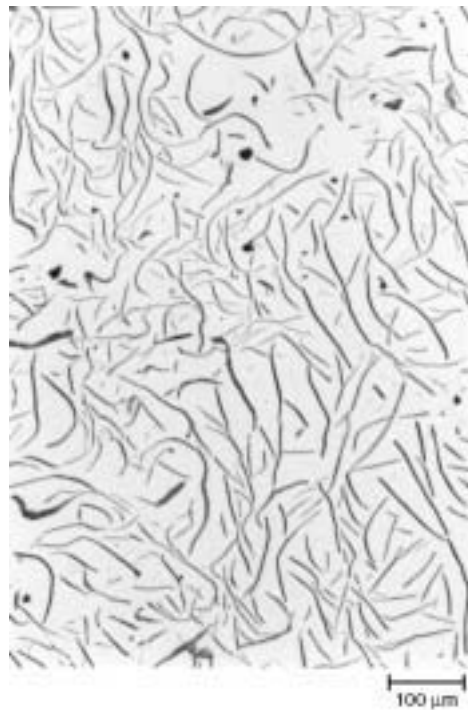


**Fig. 60** Hypereutectic as-cast gray iron (Fe-3.5%C-2.95%Si-0.4%Mn-0.08%P-0.02%S-0.13%Ni-0.15%Cu). Flake graphite type A. As-polished. 100×

**Table 3** Constituents commonly found in cast iron microstructures, and their general effect on physical properties

Constituent	Characteristics and effects
Graphite (hexagonal crystal structure)	Free carbon; soft; improves machinability and damping properties; reduces shrinkage and may reduce strength severely, depending on shape
Austenite ( $\gamma$ -iron)	Face-centered cubic crystal structure. The character of the primary phase, which solidifies from the oversaturated liquid alloy in dendrite form, is maintained until room temperature. Austenite is metastable or stable equilibrium phase (depending upon alloy composition). Usually transforms into other phases. Seen only in certain alloys. Soft and ductile, approximately 200 HB
Ferrite ( $\alpha$ -iron)	Body-centered cubic crystal structure. Iron with elements in solid solution, which is a stable equilibrium, low-temperature phase. Soft, 80–90 HB; contributes ductility but little strength
Cementite ( $\text{Fe}_3\text{C}$ )	Complex orthorhombic crystal structure. Hard, intermetallic phase, 800–1400 HV depending upon substitution of elements for Fe; imparts wear resistance; reduces machinability
Pearlite	A metastable lamellar aggregate of ferrite and cementite due to eutectoidal transformation of austenite above the bainite region. Contributes strength without brittleness; has good machinability, approximately 230 HB
Martensite	Generic term for microstructures that form by diffusionless transformation, where the parent and product phases have a specific crystallographic relationship. Hard metastable phase
Steadite (phosphorous eutectic)	A pseudobinary or ternary eutectic of ferrite and iron phosphide or ferrite, iron phosphide, and cementite, respectively. It can form in gray iron or in mottled iron with a phosphorous content >0.06%. Hard and brittle; solidifies from the liquid on cooling at the cell boundaries as a last constituent of the microstructure
Ledeburite	Massive eutectic phase composed of cementite and austenite; austenite transforms to cementite and pearlite on cooling. Produces high hardness and wear resistance; virtually unmachinable

Source: Ref 3, 10

Features that are perpendicular to the optic axis in BFI appear white, while in DFI they are black. Likewise, features that are at an angle to the surface, such as grain boundaries and phase boundaries, appear black in BFI but are white (self-luminous in appearance) in DFI.

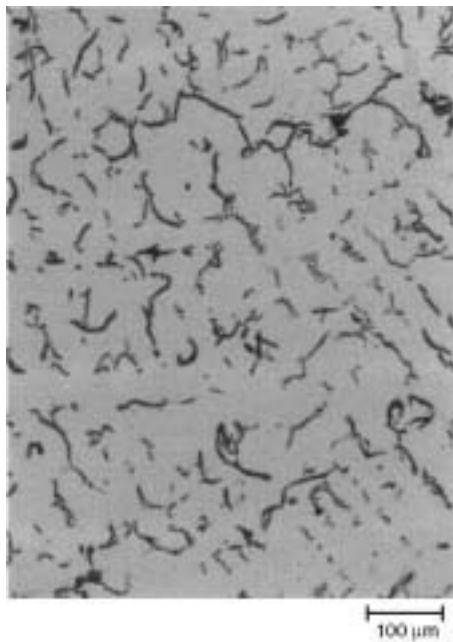


**Fig. 61** Hypereutectic as-cast gray iron (Fe-2.18% C, 2.49% Si-0.7% Mn-0.06% P-0.05% S). Flake graphite type E. As-polished. 100 $\times$ . Courtesy of G.F. Vander Voort, Buehler Ltd.



**Fig. 62** Hypereutectic as-cast gray iron (Fe-3.3% C, 2.75% Si-0.88% Mn-0.42% P-0.086% S). Flake graphite type B. As-polished. 90 $\times$  (microscopic examination 100 $\times$ )

When crossed polarized light is used along with a double-quartz prism (Wollaston prism) placed between the objective and the vertical illuminator, two light beams are produced that ex-

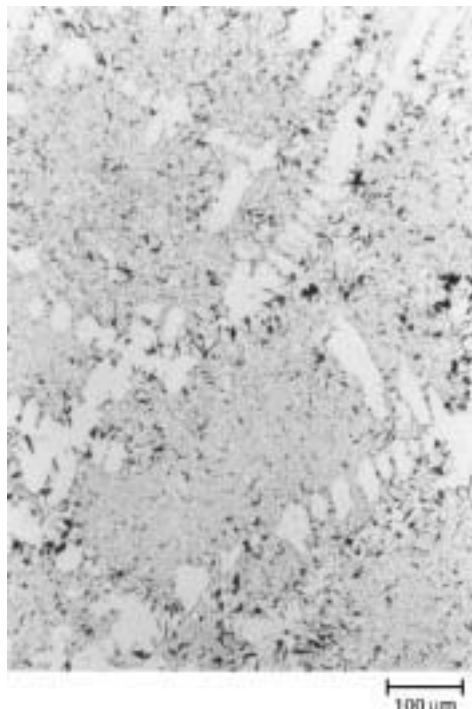


**Fig. 63** Hypereutectic as-cast gray iron (Fe-3.4% C, 3.4% Si-0.07% Mn-0.04% P-0.03% Cr-0.47% Cu). Pointlike flake graphite type D. As-polished. 100 $\times$

hibit coherent interference in the image plane. This leads to two slightly displaced (laterally) images differing in phase ( $\lambda/2$ ), which produces higher contrast for nonplanar detail. This is called differential interference contrast (DIC), and the most common system is the one developed by Nomarski. The image reveals topographic detail somewhat similar to that produced by oblique illumination but without the loss of resolution. Images can be viewed with natural colors similar to those observed in bright field, or artificial coloring can be introduced by adding a sensitive tint plate (Ref 4).

The microstructure of Fe-Cr-Mn cast irons can be examined in DIC after polishing. Figure 45 shows the microstructure of the high-chromium cast iron (shown previously in Fig. 43 and 44) but as-polished (unetched) and examined in DIC. The chromium carbides, which are much harder than the matrix, stand above it in relief and can be seen very well.

The DFI and DIC methods also can be used for revealing the details of microstructures in alloyed irons, for example, a chromium-nickel iron after heat treatment, which were barely visible after etching with nital. Figures 46 to 48 show the microstructure of the Fe-Cr-Ni alloyed iron after heat treatment and after etching with 4% nital, but for a shorter time than usual. The three micrographs show the results for the same field after examination with BFI, DFI, and DIC, respectively. The BFI image reveals the martensite poorly, and the secondary carbides are barely visible. However, both the DFI and DIC images reveal the martensite, although not strongly,

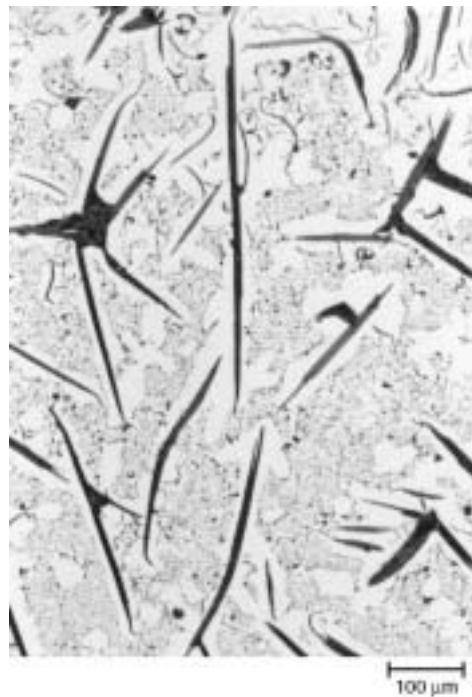


**Fig. 64** Hypereutectic as-cast gray iron (Fe-4.3% C, 1.5% Si-0.5% Mn-0.12% P-0.08% S). Flake graphite type C (kish graphite). As-polished. 100 $\times$

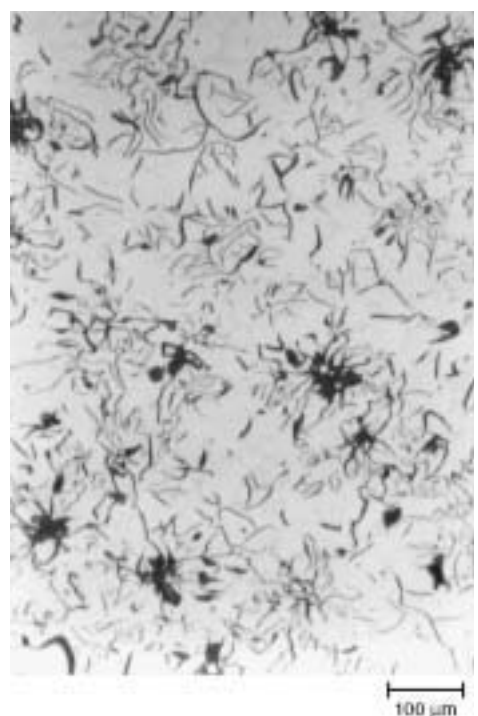
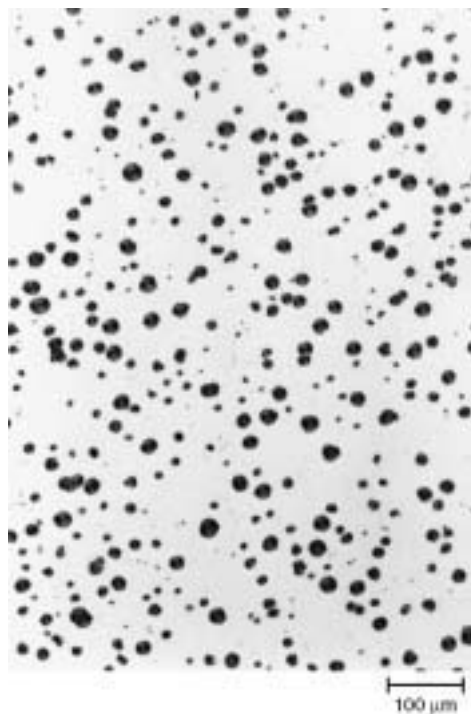


**Fig. 65** As-cast gray iron. Flake graphite type V (star-like graphite). As-polished. 100 $\times$

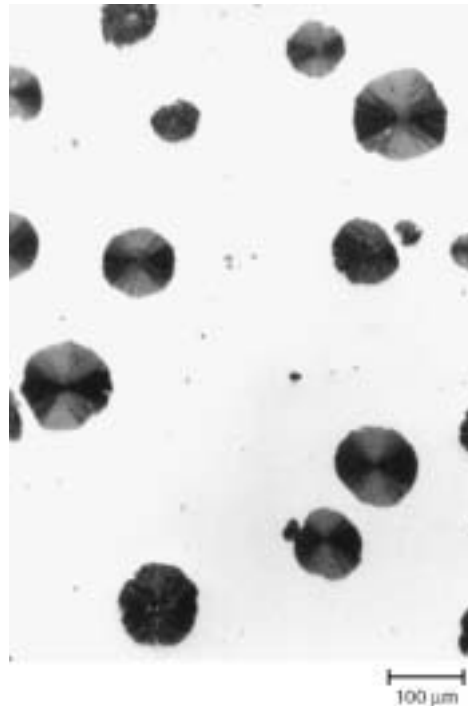
while the secondary carbides are very distinct (see also Fig. 39, 40).

The microstructure of an Fe-C-Cr cast iron after heat treatment, revealed with glyceregia and

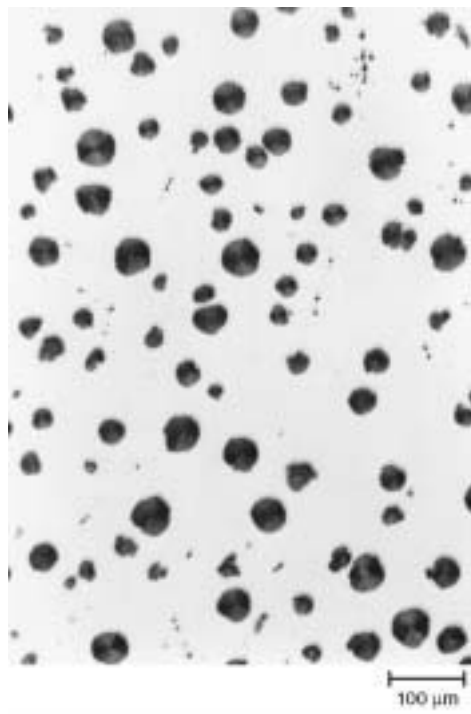
examined with BFI and DFI, is shown in Fig. 49 and 50, respectively. The details of the microstructure were revealed much more strongly with DFI than with BFI.



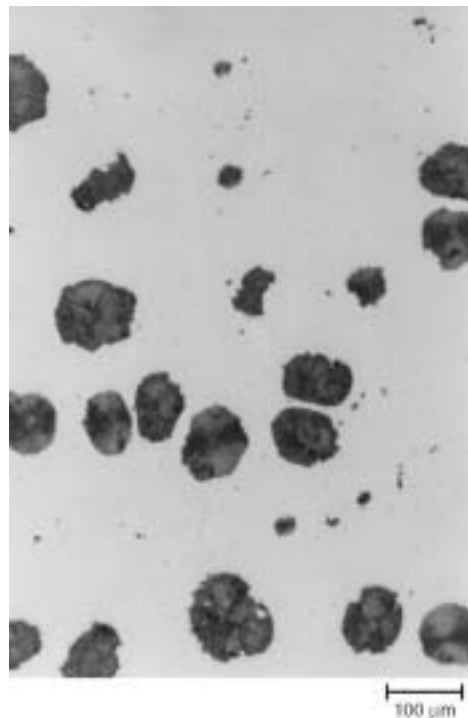
**Fig. 66** As-cast ductile iron (Fe-3.45%C-2.25%Si-0.30%Mn-0.04%P-0.01%S-0.8%Ni-0.07%Mg-0.55%Cu). Nodular graphite size is 20  $\mu\text{m}$ . As-polished. 100 $\times$



**Fig. 68** As-cast ductile iron. Nodular graphite size is 100  $\mu\text{m}$ . As-polished. 100 $\times$



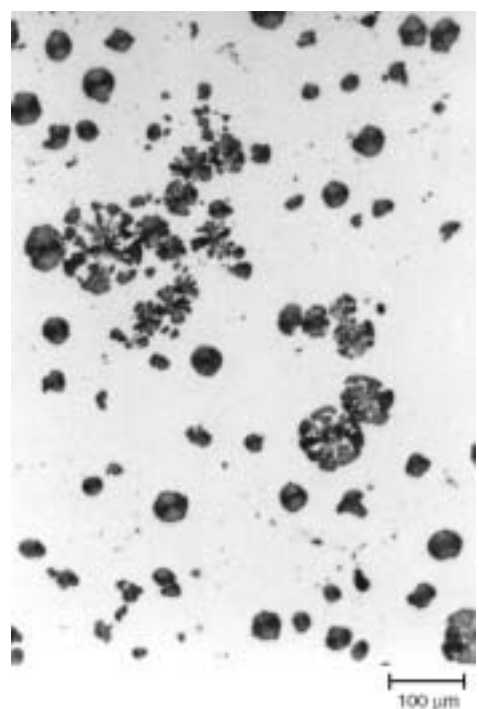
**Fig. 67** As-cast ductile iron (Fe-3.6%C-2.9%Si-0.14%Mn-0.04%P-0.02%S-0.16%Ni-0.06%Mg). Nodular graphite size is 40  $\mu\text{m}$ . As-polished. 100 $\times$



**Fig. 69** As-cast ductile iron. Imperfectly formed graphite nodules. As-polished. 100 $\times$

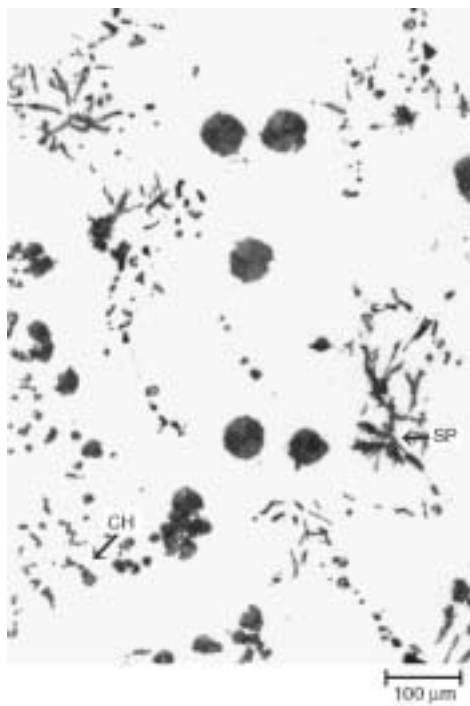
**Polarized Light Response.** Polarized light is obtained by placing a polarizer (usually a Polaroid filter, Polaroid Corp.) in front of the condenser lens of the microscope and placing an analyzer (another Polaroid filter) before the eyepiece. The polarizer produces plane-polarized light that strikes the surface and is reflected through the analyzer to the eyepieces. If an anisotropic metal is examined with the analyzer set 90° to the polarizer, the grain structure will be visible. However, viewing of an isotropic metal (cubic metals) under such conditions will produce dark, extinguished conditions (complete darkness is not possible using Polaroid filters). Polarized light is particularly useful in metallography for revealing grain structures and twinning in anisotropic metals and alloys as well as for identifying anisotropic phases and inclusions. This method also improves the contrast of microstructures, providing more structural details (Ref. 4).

Figure 51 shows the microstructure of a graphite nodule in BFI, while Fig. 52 shows the same nodule in crossed polarized light. Polarized light reveals much better than BFI the radial structure of the graphite nodule that grows from the central nucleus. Also, the cross, which is characteristic of the perfectly formed graphite nodule, can be made visible only with the use of this technique. Figure 53 shows the anisotropic layered structure of graphite flakes, which also respond to polarized light. In both cases, the colors of graphite vary due to the anisotropy of graphite. Figure 54 shows the microstructure of ADI, consisting of martensite and a small



**Fig. 70** As-cast ductile iron. Exploded graphite. As-polished. 100 $\times$

amount of acicular ferrite. The specimen was etched with 4% picral to reveal the acicular ferrite in the background of the almost invisible martensite (see Fig. 33). When examination was carried out with crossed polarized light plus a



**Fig. 71** Austempered ductile iron (Fe-3.6%C-2.5%Si-0.052%Mg-0.7%Cu). Chunky (CH) and spiky (SP) types of graphite. As-polished. 100×



**Fig. 72** As-cast iron with compacted graphite (Fe-3.7%C-2.3%Si-0.21%Mn-0.03%P-0.01%S-0.82%Ni-0.02%Mg). Graphite size is 80 to 160 μm. As polished. 100×

sensitive tint filter, shown in Fig. 54, the ferritic needles can be seen by shining with a white color. Also, many of the coarsest martensitic plates (body-centered tetragonal crystal structure) with the proper lattice orientation were visible in polarized light but barely visible in BFI.

## Microstructures

Table 3 lists the characteristics of typical constituents of cast iron microstructures and their effect on mechanical properties (Ref 3, 10).



**Fig. 73** Malleable iron (Fe-2.65%C-1.2%Si-0.53%Mn-0.06%P-0.21%S-0.08%Cr-0.10%Cu-0.07%Ni-<0.01%Al). Temper graphite type III with maximum size of 80 μm. As-polished. 100×

## Microstructure of Graphite

The eutectic graphite cell has a continuous graphite skeleton, but on the metallographic cross section, the three-dimensional nature is not obvious. Figures 55 to 57 show scanning electron microscopy (SEM) micrographs of flake, nodular, and compacted graphite, respectively. Contrary to flake graphite, where the flakes solidify as an aggregate and each such agglomeration is one eutectic cell, both spheroidal and compacted graphite solidify as separate precipitates. For SEM examination, the specimens were deeply etched (Table 2, etch No. 13).

Characteristic properties of graphite precipitations are shape, size, and distribution. There is a correlation between different graphite morphologies, the chemical composition, and the cooling rate.

**Flake Graphite in Gray Iron.** Flake (lamellar) graphite is characteristic of gray iron, and components such as aluminum, carbon, and silicon promote its formation. When the cooling rate increases, the flakes get finer, and their distribution tends to be interdendritic. Figure 58 shows a hypoeutectic gray iron with a uniform distribution of randomly oriented graphite flakes with a maximum length of 320 μm (type A flake graphite in the ASTM A 247 classifications). Figure 59 shows a fine, type D flake graphite with a maximum length of 40 μm, also in a hypoeutectic alloy, but it solidified at a higher cooling rate, which promoted the interdendritic distribution. Type A graphite in a hypereutectic gray iron is shown in Fig. 60. It has the most desired shape and distribution, and it is very characteristic of gray iron casts with high machinability. The maximum length of graphite flakes is 160 μm. Figures 61 and 62 show type E and type B graphite, respectively, which occur in hypereutectic gray iron at high cooling rates. Note in Fig. 62 that each rosette group of graphite represents one eutectic cell. That type of graphite is characteristic of thin-walled castings.

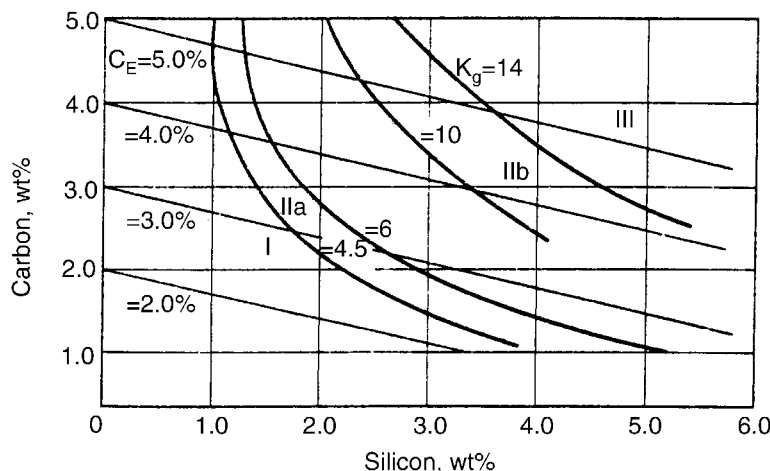


**Fig. 74** The diagram of correlation between a type of matrix in nonalloyed cast irons and silicon and phosphorus content as well as the thickness,  $R$ , of the casting wall, which relates to the cooling rate.  $K_g = C(\text{Si} + \log R)$  is a coefficient of graphitization, and  $C_E = C + \frac{1}{3}\text{Si} + \frac{1}{3}\text{P}$  is the coefficient of saturation (carbon equivalent). Region I is white cast iron (pearlite, cementite, no graphite); Region IIa is mottled cast iron (pearlite, graphite, cementite); Region IIb is ferritic-pearlitic cast iron; Region III is ferritic cast iron. Source: Ref 13

A high degree of undercooling of hypereutectic gray iron can promote the solidification of very fine, pointlike type D graphite with an interdendritic distribution, as shown in Fig. 63. In the other direction, undertreatment of the graph-

itizing inoculants, such as ferrosilicon, produces other flake graphite types in gray iron. For example, Fig. 64 shows a hypereutectic gray iron with graphite type C, where very coarse, needle-

like flakes (kish graphite) form before the eutectic, which is very fine. Kish graphite, which is shown in Fig. 64, can be changed into a starlike graphite, shown in Fig. 65, under higher cooling rates, which is referred to as type V (plate I of ASTM A 247). The carbide-forming alloy elements, for example, chromium, manganese, and vanadium, and the low-melting-point metals, for example, bismuth, lead, and sulfur, also affect graphite morphology.

**Nodular Graphite in Ductile Iron.** The addition of magnesium in the inoculation process desulfurizes the iron and makes graphite precipitate as nodules rather than flakes. Moreover, mechanical properties are greatly improved over gray iron; hence, nodular iron is widely known as ductile iron. Nodule size and shape perfection can vary, depending on composition and cooling rate. Figure 66 shows fine nodules with a maximum diameter of 20  $\mu\text{m}$  in a chill-cast thin section, while Fig. 67 and 68 show coarser nodules, with maximum diameters of 40 and 100  $\mu\text{m}$ , respectively. Note that the number of nodules per unit area is different and changes from approximately 350 to 125 to 22/ $\text{mm}^2$ , respectively, for Fig. 66 to 68.

Certain factors can cause weak nodularity. Figure 69 shows an irregular graphite shape due to poor inoculation or excessive fading of inoculant. Exploded graphite, shown in Fig. 70, may occur due to excessive rare earth additions. Normally, it is found in thick-section castings or at higher-carbon equivalents (Ref 11). Figure 71 shows chunky and spiky types of graphite. The first one is caused by high-purity charge mate-

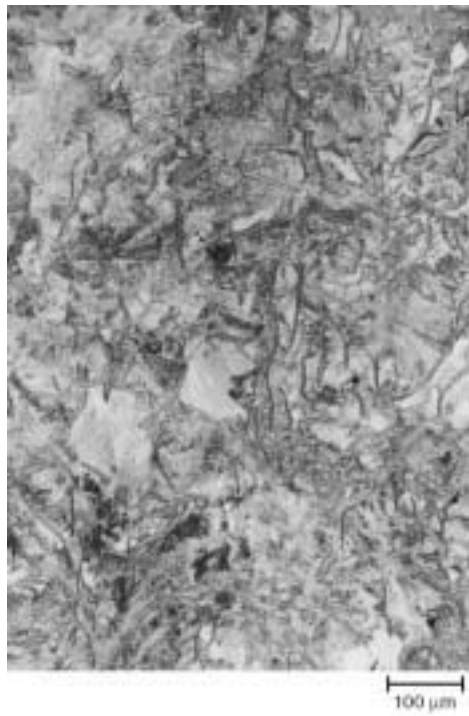


**Fig. 75** As-cast gray iron (Fe-2.8% C-1.85% Si-1.05% Mn-0.04% P-0.025% S). Pearlitic matrix. Etched with 4% nital. 100 $\times$



**Fig. 77** As-cast gray iron. Pearlitic-ferritic matrix with phosphorous eutectic (E). Etched with 4% nital. 100 $\times$



**Fig. 76** Same as in Fig. 75. Fine pearlite. 500 $\times$



**Fig. 78** Same as in Fig. 77. E, ternary phosphorous eutectic; P, pearlite; and F, ferrite. 500 $\times$

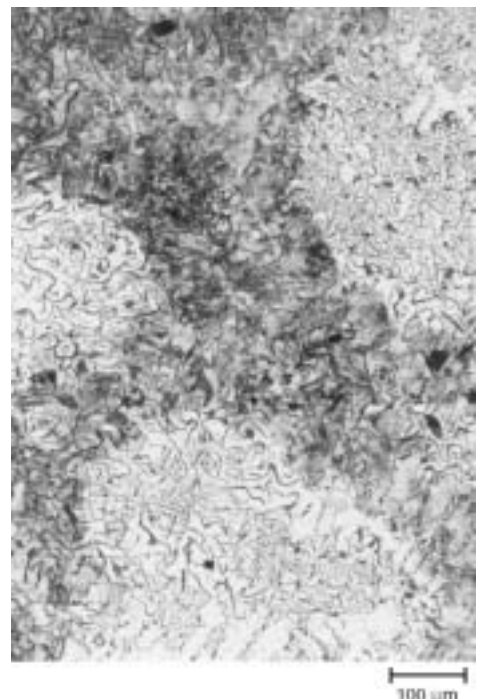


**Fig. 79** As-cast gray iron (Fe-3.4% C-3.4% Si-0.07% Mn-0.04% P-0.03% Cr-0.47% Cu). Ferritic-pearlitic matrix. Etched with 4% nital. 100 $\times$

rials and excess rare earth additions in high-carbon-equivalent compositions, while the second one is caused by small amounts of tramp elements, for example, lead, bismuth, tin, and titanium, in the absence of cerium (Ref 12).

**Compacted Graphite.** Methods that produce compacted graphite cast iron include the treatment of molten iron with rare earth inoculants, adding a lower amount of magnesium than is required to obtain nodular graphite, or adding

elements such as titanium and aluminum that make it difficult to spheroidize graphite. This type of iron is a more recent development, made in an effort to improve the mechanical properties of flake gray iron. Figure 72 shows an example

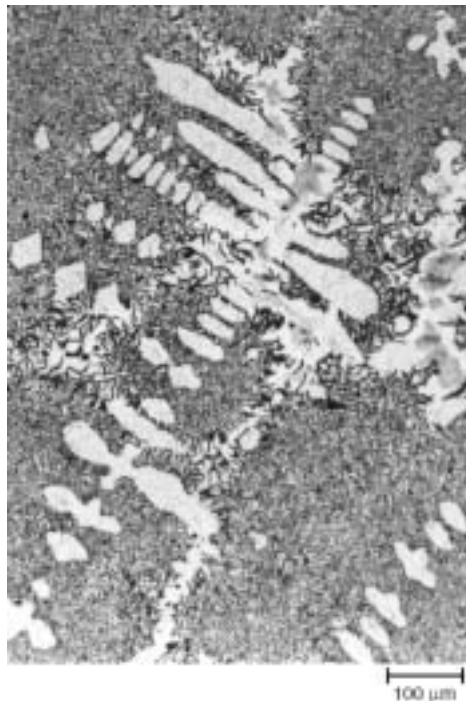


**Fig. 80** As-cast gray iron (Fe-3.4% C-3.2% Si-0.09% Mn-0.04% P-0.01% S-0.86% Cu-<0.01% Mg). Ferritic matrix. Etched in 4% nital. 100 $\times$

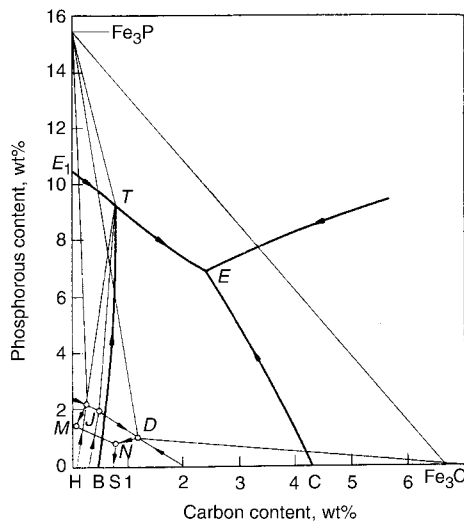


**Fig. 81** The Fe-C-P equilibrium diagram. The x-axis is the carbon content, and the y-axis is the phosphorus content. Source: Ref 13

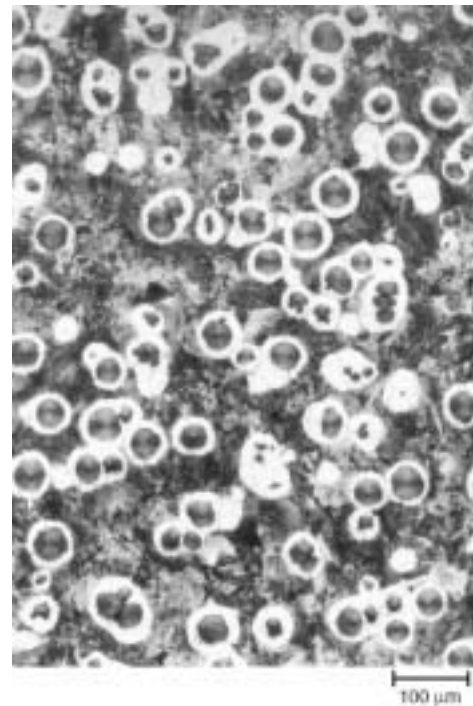


**Fig. 82** As-cast ductile iron (Fe-3.7% C-1.25% Si-0.03% Mn-0.02% P-0.02% S-0.24% Ni-0.06% Mg). Pearlite matrix with ferritic halos around graphite nodules. Etched with 4% nital. 100 $\times$

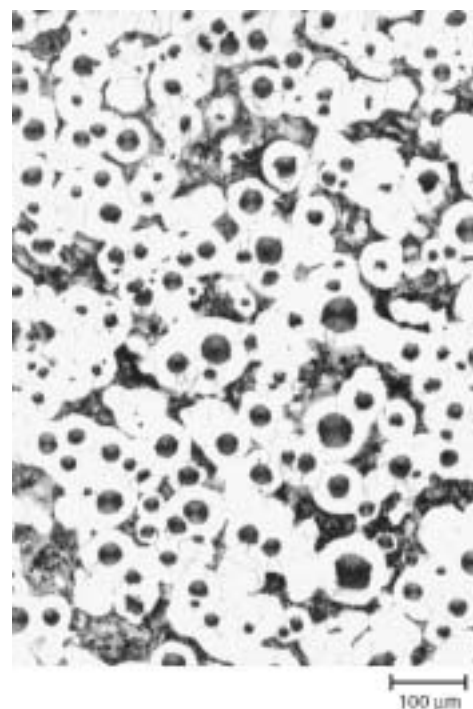


**Fig. 83** As-cast ductile iron. Ferritic-pearlitic matrix. Etched with 4% nital. 100 $\times$

where the longest compacted graphite precipitations are in the 80 to 160  $\mu\text{m}$  range.

**Temper Graphite in Malleable Iron.** Temper graphite is formed by annealing white cast iron castings to convert carbon in the form of cementite to graphite, called temper-carbon nodules. Figure 73 shows the type III graphite precipitation with 80  $\mu\text{m}$  maximum size.

#### Microstructure of Matrix

The matrix of gray, nodular, compacted, and malleable cast irons can be pearlitic, pearlitic-ferritic, ferritic-pearlitic, or ferritic. The same matrix constituents can be present in white cast iron, but cementite precipitates from the melt, rather than graphite, due to crystallization in a metastable system.

The matrix microstructure depends on chemical composition as well as on the temperature of the eutectoidal transformation. Figure 74 shows the diagram of the correlation between the type of matrix in nonalloyed cast irons and the silicon and phosphorus content as well as the thickness,  $R$ , of the casting wall, which relates to the cooling rate.  $K_g = C(\text{Si} + \log R)$  gives the coefficient of graphitization, and  $C_E = C + \frac{1}{3}\text{Si} + \frac{1}{3}\text{P}$  is the coefficient of saturation (carbon equivalent). A low value of  $K_g$  promotes solidification of white cast iron, with cementite and pearlite as the microstructure, regardless of the total carbon content,  $C$ . When the  $K_g$  coefficient and the silicon content increase, the microstruc-

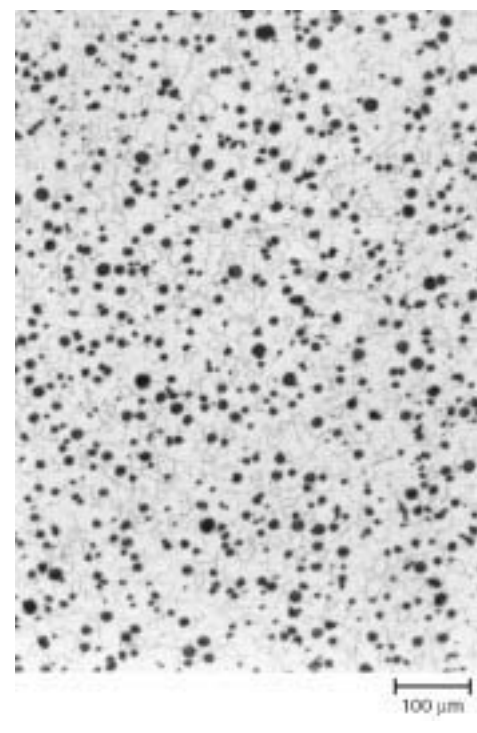


**Fig. 84** Ductile iron. Ferritic matrix. The casting was annealed at 900 °C (1650 °F), held 2 h, quick furnace cooled to 730 °C (1345 °F), slow furnace cooled to 600 °C (1110 °F), and air cooled. Etched with 4% nital. 100 $\times$

ture of the cast iron matrix tends to be pearlitic through pearlitic-ferritic to ferritic, and it depends on the  $C_E$  value (Ref 13).

In pearlitic-ferritic cast irons, the regions with ferrite always occur within the eutectic cells and

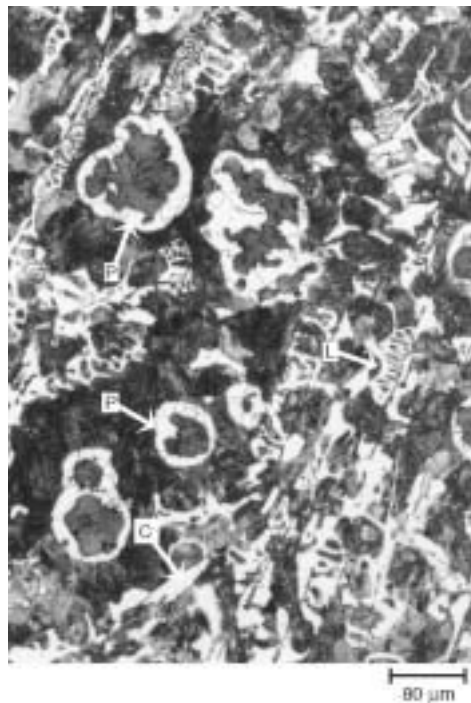


**Fig. 85** As-cast ductile iron (Fe-3.35% C-2.05% Si-0.08% Mn-0.04% P-0.02% Cr-0.02% Ni-0.045% Mg). C, cementite; L, ledeburite; and P, pearlite and ferrite around graphite nodules. Etched with 4% nital. 125 $\times$  (microscopic magnification is 100 $\times$ )

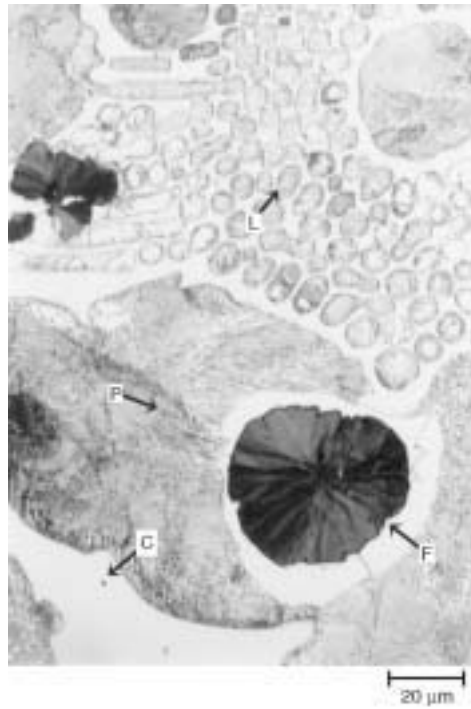


**Fig. 86** Same as in Fig. 85. C, cementite; L, ledeburite; F, ferrite; and P, pearlite. 500 $\times$

in the neighborhood of graphite precipitates due to microsegregation. The microregions of solidification, like the axis of dendrites and the interiors of eutectic cells, contain more silicon, which promotes ferrite formation. Slow cooling, as well as higher silicon contents, usually produces ferrite, while a very fast cooling rate can produce free cementite. Ferritic microstructures also can be obtained by annealing of pearlitic cast irons or in thick-walled castings (Ref 13).

**Gray iron** is classified according to minimum tensile strength of the test bars. The matrix is predominantly pearlitic (Fig. 75, 76) but also can be pearlitic-ferritic (Fig. 77, 78), ferritic-pearlitic (Fig. 79), or ferritic (Fig. 80).

A common characteristic constituent of gray iron microstructures is the phosphorus eutectic known as steadite. Figure 81 shows the Fe-C-P equilibrium diagram, while Table 4 shows the transformations that occur in this system during

solidification as well as in the solid state. The characteristic property of this system is a large area of the ternary phosphorous eutectic due to the strong tendency for phosphorus to segregate. This type of eutectic appears in the microstructure of cast irons already at 0.07% P (Ref 13).

The form of the phosphorus eutectic depends on the chemical composition of the gray iron. In irons with an average tendency to graphitization and a phosphorus content of approximately 0.4%, the fine-grain ternary eutectic solidifies from the liquid and consists of ferrite +  $Fe_3P$  +  $Fe_3C$ . In gray iron with a strong tendency for cementite solidification and with carbide-forming elements, the ternary eutectic may also contain large columnar precipitates of cementite.

Increasing the amount of strong graphitizing elements, such as silicon, promotes solidification of the binary phosphorous eutectic, ferrite +  $Fe_3P$  +  $C_{gr}$ , instead of the ternary one. The bi-

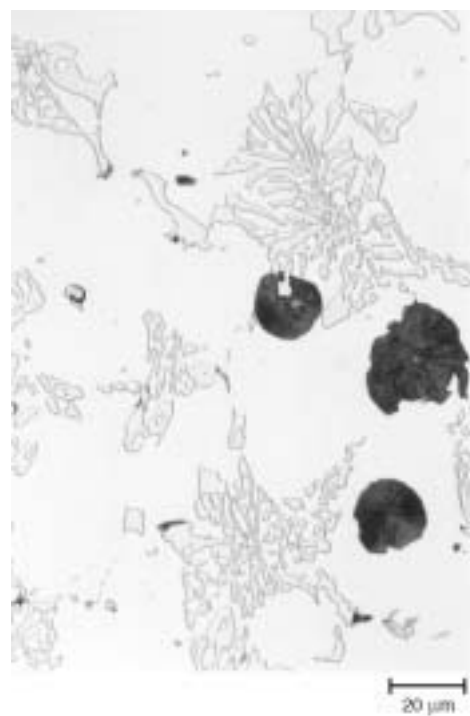


**Fig. 87** As-cast austenitic ductile iron (Fe-2.7% C-2.85% Si-1.15% Mn-0.03% P-0.01% S-2.8% Cr-20.0% Ni-0.1% Mg). Austenite and eutectic carbides type  $M_7C_3$ . Etched with glyceregia. 500 $\times$



**Fig. 88** Austempered ductile iron (the same ductile iron as in Fig. 32). Acicular ferrite and austenite. The casting was austempered: 900 °C (1650 °F), held 2 h, taken to salt bath at 360 °C (680 °F), held 180 min, and air cooled. Etched with 4% nital. 500 $\times$

**Table 4 Transformations in the range of solidification and in the solid state according to the Fe-C-P diagram (Fig. 81)**

Symbol on the Fe-C-P diagram	Transformation(a)	Type of transformation	Temperature	Composition of phases(b)
TJ	$L + \alpha \leftrightarrow \gamma + Fe_3P$	Peritectic	1005 °C (1840 °F)	L = 0.8 C, 9.2% P α = 0.3% C, 2.2% P γ = 0.5% C, 2.0% P
E	$L \leftrightarrow \gamma + Fe_3P + Fe_3C$	Eutectic	950 °C (1740 °F)	L = 2.4% C, 6.89% P γ = 1.2% C, 1.1% P
MN	$\gamma + Fe_3P \leftrightarrow \alpha + Fe_3C$	Peritectoidal	745 °C (1375 °F)	γ = 0.8% C, 1.0% P α = 0.1% C, 1.5% P

(a) L, melt (liquid metal); α, ferrite (α-iron); γ, austenite (γ-iron);  $Fe_3P$ , iron phosphide;  $Fe_3C$ , cementite. (b) Maximum solubility of chemical components in the particular phases. Source: Ref 13

nary eutectic is called a pseudobinary eutectic, because carbon is removed from the eutectic during diffusion in the solid state (Ref 13).



**Fig. 89** Austempered ductile iron (the same composition as in Fig. 32). Acicular ferrite and austenite. The casting was austempered: 900 °C (1650 °F), held 2 h, taken to salt bath at 380 °C (715 °F), held 180 min, and air cooled. Etched with 4% nital. 500×

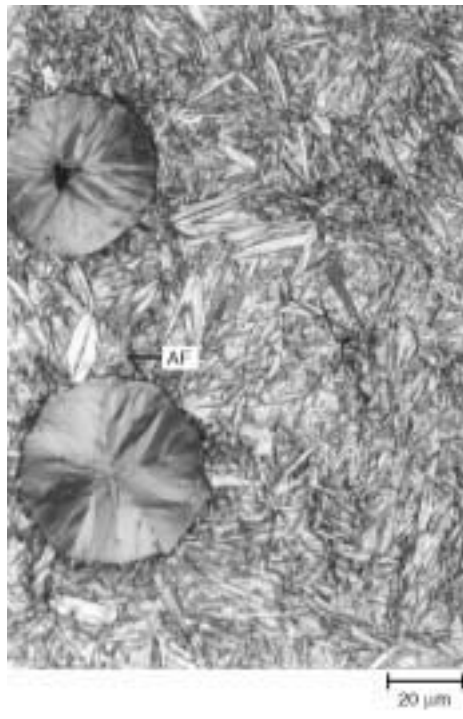


**Fig. 90** Austempered ductile iron (the same composition as in Fig. 32). Martensite and small amount of acicular ferrite (AF). The casting was austempered: 900 °C (1650 °F), held 2 h, taken to salt bath at 300 °C (570 °F), held 2 min, and air cooled. Etched with 4% nital. 1000×

**Ductile iron** microstructures normally consist of pearlite or pearlite and ferrite with graphite nodules surrounded with ferrite, which look like a white halo, although the more common name of this structure is the bull's-eye structure. Figures 82 and 83 show this type of microstructure, while Fig. 84 shows a fully ferritic-matrix microstructure that was achieved after annealing a chilled casting with a microstructure containing cementite, ferrite, and pearlite (see also Fig. 11). In some cases, usually at a high cooling rate, cementite occurs as a separate constituent in the matrix.

The precipitates of cementite are situated in the exterior regions of the eutectic cells or in the interdendritic spaces of the transformed austenite due to the microsegregation of carbide-forming elements, such as manganese, chromium, or vanadium. Cementite appears very frequently in chill castings or in thin-walled sand castings (Ref 13). Figures 85 and 86 show the microstructure of pearlitic ductile iron with cementite and ledeburite. In this case, cementite was a desired constituent of the microstructure to improve the wear resistance of cast iron. It was achieved by feeding the melted metal with an iron-magnesium foundry alloy, without inoculation. The graphite nodules do not have a perfect shape. Figure 87 shows the microstructure of a heat- and wear-resistant ductile iron containing chromium and nickel, which consists of chromium carbides in an austenitic matrix.

The austempering heat treatment is used to achieve better mechanical properties in ductile

iron. The casting is heated to a temperature range of 840 to 950 °C (1545 to 1740 °F) and held at this temperature until the entire matrix is transformed to austenite saturated with carbon. The casting is then quenched rapidly to austempering temperature, between 230 and 400 °C (445 and 750 °F), and held at this temperature for the required time (Ref 14). When this cycle is properly performed, the final structure of the matrix, which is called ausferrite, consists of acicular ferrite and austenite, and the iron is called austempered ductile iron (ADI). The morphology and amount of ferrite depends on the time and temperature of the austempering process. Figures 88 and 89 show an ADI microstructure after austempering heat treatment, when the casting in both cases was held in the furnace for 180 min, and the annealing temperatures were different. The use of a higher temperature changed the morphology of the ferrite and increased the amount of austenite. Figure 90 shows the ADI microstructure after 2 min austempering heat treatment, when the transformation of austenite to acicular ferrite was just started, so martensite is the dominant phase, and there is only a small amount of acicular ferrite, mostly surrounding the graphite nodules (see also Fig. 31 to 37).

**Compacted graphite-iron** matrix microstructures consist of ferrite and pearlite; the amount of each constituent depends on the cooling rate and the chemical composition (elements that promote either ferrite or pearlite solidifica-

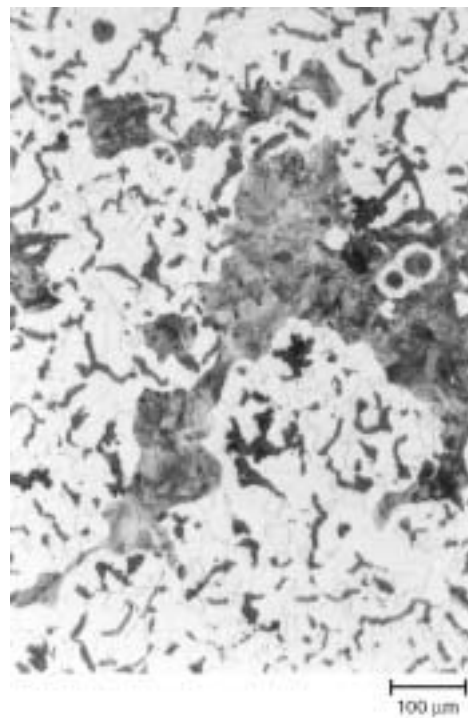


**Fig. 91** As-cast iron with compacted graphite (Fe-2.8%C-1.9%Si-0.55%Mn-0.04%P-0.2%S-0.018%Mg). Ferritic-pearlitic matrix. Etched with 4% nital. 1000×

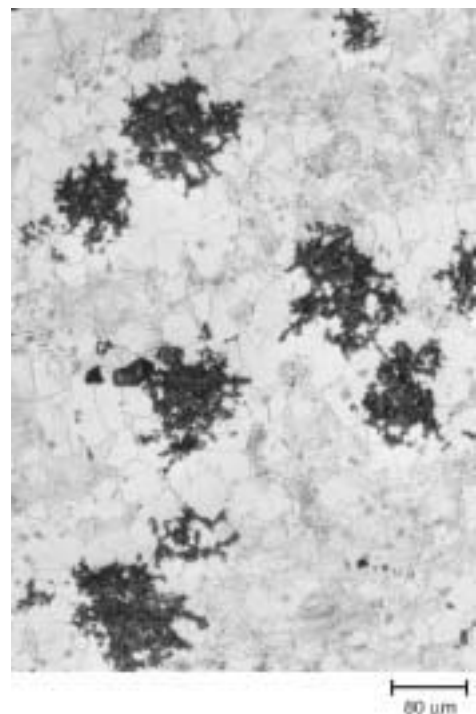


**Fig. 92** Malleable iron (Fe-2.95%C-1.2%Si-0.53%Mn-0.06%P-0.21%Si-0.08%Cr-0.10%Cu-0.07%Ni-<0.01%Al). The casting was annealed: at 950 °C (1740 °F), held 10 h, furnace cooled to 720 °C (1330 °F), held 16 h, and air cooled. Pearlitic-ferritic matrix. Etched with 4% nital. 125× (microscopic magnification 100×)

tion). Figure 91 shows a ferritic-pearlitic microstructure with a small amount of nodular graphite.

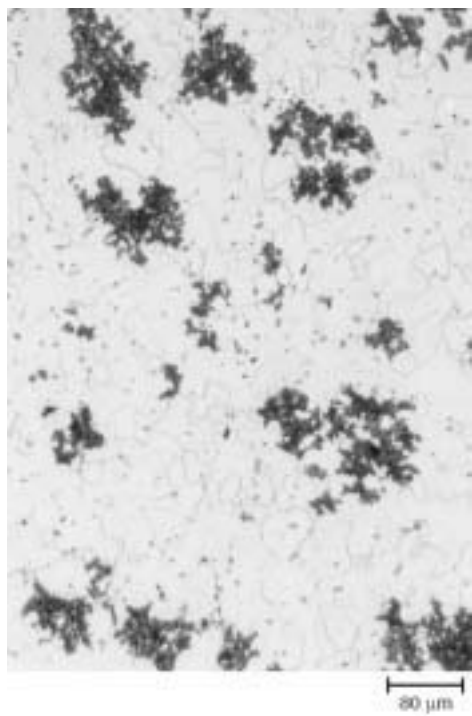


**Fig. 93** Malleable iron (Fe-2.9%C-1.5%Si-0.53%Mn-0.06%P-0.22%S-0.09%Cr-0.10%Cu-0.08%Ni-0.02%Al). The casting was annealed as in Fig. 92. Ferrite. Etched with 4% nital. 125 $\times$  (microscopic magnification 100 $\times$ )



**Fig. 94** As-cast white iron (Fe-3.0%C-2.7%Si-0.45%Mn-0.07%P-0.025%S). C, cementite; P, pearlite. Etched with 4% nital. 400 $\times$

**Malleable iron** matrix microstructures are mostly ferritic, ferritic-pearlitic, or pearlitic, depending on the cast-making process used. The type of matrix is a result of transformation in the solid state during the annealing of white cast iron. Figures 92 and 93 show the microstructure

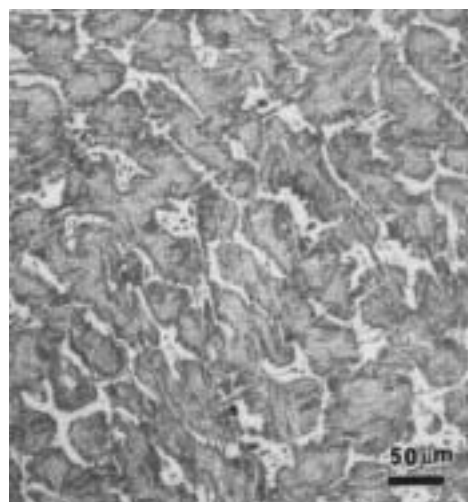


**Fig. 95** White cast iron after heat treatment. A network of massive cementite and tempered martensite. Etched with 4% picral. 140 $\times$ . Courtesy of G.F. Vander Voort, Buehler Ltd.

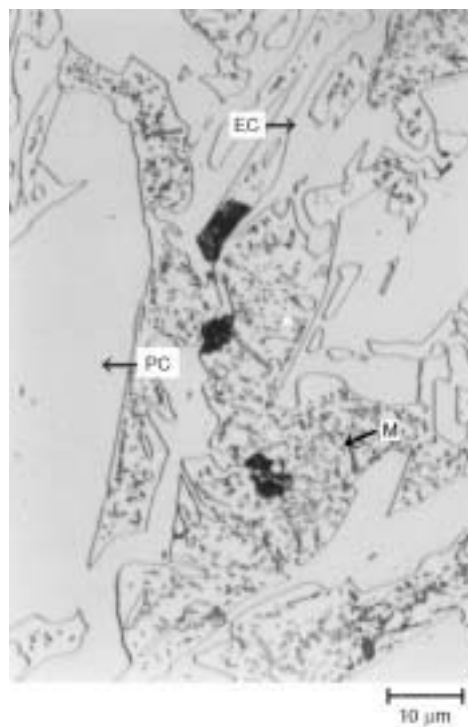


**Fig. 96** White high-chromium cast iron (see Fig. 43). PC, primary carbides; EC, eutectic carbides in martensitic matrix with fine, globular secondary carbides. The casting was heat treated at 1000 °C (1830 °F), held 1 h, furnace cooled to 550 °C (1020 °F), held 4 h in a 400 °C (750 °F) salt bath, and air cooled. Etched with glycerceria. 1000 $\times$

of the pearlitic-ferritic and ferritic malleable iron, respectively. The annealing process was the same one in both cases, but the final microstructures were achieved by the use of different foundry processes. In the case of the pearlitic-ferritic microstructure, the inoculation and deoxidation processes were not carried out. When these two processes were used, that is, deoxidation with aluminum and inoculation with iron-silicon and pure bismuth, the result was a ferritic microstructure after annealing.

**Unalloyed white iron microstructures** are created when the castings solidify in the metastable system and the structure is free of graphite. The matrix may consist of cementite and pearlite, as shown in Fig. 94, or, after heat treatment, of cementite and martensite, as shown in Fig. 95. This type of white iron belongs to the class of abrasion-resistant cast irons and usually is produced as chill castings.

**High-chromium white iron** is a type of highly wear-resistant iron with a microstructure that consists of primary and eutectic carbides, for example,  $(FeCr)_3C$ ,  $(FeCr)_7C_3$ , and  $(FeCr)_{23}C_6$ , depending on the chemical composition and cooling rate during solidification. The primary carbides have a typical shape, which in cross section is similar to the letter "L," and have the chemical formula  $M_3C$  at higher cooling rate and low chromium content. When the cooling rate slows down and the chromium content increases to, for example, 30% and higher, the primary chromium carbides have a hexagonal shape with a characteristic hole in the center. The eutectic carbides are always type  $M_7C_3$ , independent of chromium content and cooling rate (Ref 15).

The type  $M_{23}C_6$  carbides solidify when the chromium content is approximately 50 to 60% (Ref 16). The same factors that affect the type of carbides also influence the type of matrix, which can be austenitic but also ferritic or pearlitic. When the cooling rate is respectively slow, secondary precipitations can occur around the austenitic dendrites (Ref 17).

It has been proven that the annealing heat treatment destabilizes the matrix, which will transform into either bainite or martensite with small secondary carbide precipitates. The resulting transformation product is a function of the cooling rate from annealing as well as the chemical composition; for example, when  $Cr/C < 5$ , the matrix microstructure was bainitic, while exceeding this value produced martensitic transformation (Ref 18). Figure 96 shows the microstructure of high-chromium white cast iron after isothermal heat treatment; the secondary, fine carbides precipitated from the austenitic matrix, which transformed into martensite (see also Fig. 43, 44, and 45).

#### ACKNOWLEDGMENTS

For samples and examination results, many thanks to:

- Colleagues at the Foundry Research Institute, Kraków, Poland: Adam Kowalski, W. Wierz-

- chowski, J. Turzyński, W. Madej, K. Głównia, A. Pytel, and J. Bryniarska
- M. Sorochtej of The Kraków Technical University

Also, many thanks to M. Warmuzek at the Foundry Research Institute for making the SEM micrographs of different types of graphite.

Special thanks to G.F. Vander Voort from Buehler Ltd. for his advice and help in preparing this article.

## REFERENCES

1. Guide to Engineered Materials, Property Comparison Tables, *Adv. Mater. Process.*, Vol 159 (No. 12), Dec 2001, p 46
2. Cz. Podrzucki and Cz. Kalata, *Metalurgia i odlewictwo żeliwa (Metallurgy and Foundry of Cast Iron)*, Śląsk-Katowice, Poland, 1971, p 32, 54–59, 70
3. W. Sakwa, *Żeliwo (Cast Iron)*, Śląsk-Katowice, Poland, 1974, p 53
4. G.F. Vander Voort, *Metallography: Principles and Practice*, McGraw-Hill Book Co., 1984; Reprinted by ASM International, 1999, p 129, 294–303, 632, 634, 642–644, 646, 648
5. G.F. Vander Voort, Phase Identification by Selective Etching, *Applied Metallography*, G.F. Vander Voort, Ed., Van Nostrand Reinhold Co., 1986, p 1–19
6. J. Zhou, Dalian, W. Schmitz, and S. Engler, Unterschung der Gefügebildung von Gußeisen mit Kugelgraphit bei langsamer Erstarrung, *Giessereiforschung*, Vol 39 (No. 2), 1987, p 55–70
7. P. Skočovský, *Colour Contrast in Metallographic Microscopy*, Žilina (Slovak Republic), 1993, p 26
8. E. Weck and E. Leistner, *Metallographic Instructions for Color Etching by Immersion, Part II: Beraha Color Etchants and Their Different Variations*, Deutscher Verlag für Schweißtechnik, GmbH, Düsseldorf, 1983, p 51
9. P.C. Liu and C.R. Loper, Observation on the Graphite Morphology in Cast Iron, *Trans. AFS*, Vol 88, 1980, p 97
10. J.A. Nelson, Cast Irons, *Metallography and Microstructures*, Vol 9, *ASM Handbook*, American Society for Metals, 1985, p 242
11. "Poor Nodularity in Ductile Iron," Technical Information 25, Revision No. 1, Elkem ASA, Silicon Division, 2001
12. "Graphite Structures in Cast Irons," poster, Elkem ASA
13. K. Sękowski, J. Piaskowski, and Z. Wojtowicz, *Atlas struktur znormalizowanych stopek odlewniczych (Atlas of the Standard Microstructures of Foundry Alloys)*, WNT Warszawa, Poland, 1972, p 54–55, 74–77
14. B.V. Kovacs, On the Terminology and Structure of ADI, *Trans. AFS*, Vol 102, 1994, p 417–420
15. T. Ohide and G. Ogira, Solidification of High Chromium Alloyed Cast Irons, *Br. Foundryman*, Vol 76 (No. 1), 1983, p 7
16. M. Šittner, Primární kristalizace chromových litin, Čast II (Primary Solidification of the Chromium Cast Irons, Part II), *Slévárenství*, Vol 33 (No. 9), 1985, p 363
17. P. Dupin and J.M. Schissler, Etude structural de l'état brut de fontes blanches à 17% Cr, *Hommes et Fonderie*, No. 151, 1985, p 19
18. C.P. Tong, T. Suzuki, and T. Umeda, The Influence of Chemical Composition and Destabilization on Transformation Characteristics of High Chromium Cast Irons, *Imono (J. Jpn. Foundrymen's Soc.)*, Vol 62 (No. 5), 1990, p 344



**ASM International** is the society for materials engineers and scientists, a worldwide network dedicated to advancing industry, technology, and applications of metals and materials.

ASM International, Materials Park, Ohio, USA  
[www.asminternational.org](http://www.asminternational.org)

This publication is copyright © ASM International®. All rights reserved.

Publication title	Product code
ASM Handbook, Volume 9: Metallography and Microstructures	06044G

**To order products from ASM International:**

**Online** Visit [www.asminternational.org/bookstore](http://www.asminternational.org/bookstore)

**Telephone** 1-800-336-5152 (US) or 1-440-338-5151 (Outside US)

**Fax** 1-440-338-4634

**Mail** Customer Service, ASM International  
9639 Kinsman Rd, Materials Park, Ohio 44073, USA

**Email** [CustomerService@asminternational.org](mailto:CustomerService@asminternational.org)

**In Europe** American Technical Publishers Ltd.  
27-29 Knowl Piece, Wilbury Way, Hitchin Hertfordshire SG4 0SX, United Kingdom  
Telephone: 01462 437933 (account holders), 01462 431525 (credit card)  
[www.ameritech.co.uk](http://www.ameritech.co.uk)

**In Japan** Neutrino Inc.  
Takahashi Bldg., 44-3 Fuda 1-chome, Chofu-Shi, Tokyo 182 Japan  
Telephone: 81 (0) 424 84 5550

**Terms of Use.** This publication is being made available in PDF format as a benefit to members and customers of ASM International. You may download and print a copy of this publication for your personal use only. Other use and distribution is prohibited without the express written permission of ASM International.

No warranties, express or implied, including, without limitation, warranties of merchantability or fitness for a particular purpose, are given in connection with this publication. Although this information is believed to be accurate by ASM, ASM cannot guarantee that favorable results will be obtained from the use of this publication alone. This publication is intended for use by persons having technical skill, at their sole discretion and risk. Since the conditions of product or material use are outside of ASM's control, ASM assumes no liability or obligation in connection with any use of this information. As with any material, evaluation of the material under end-use conditions prior to specification is essential. Therefore, specific testing under actual conditions is recommended.

Nothing contained in this publication shall be construed as a grant of any right of manufacture, sale, use, or reproduction, in connection with any method, process, apparatus, product, composition, or system, whether or not covered by letters patent, copyright, or trademark, and nothing contained in this publication shall be construed as a defense against any alleged infringement of letters patent, copyright, or trademark, or as a defense against liability for such infringement.